Journal for ImmunoTherapy of Cancer

Downregulation of phosphoserine phosphatase potentiates tumor immune environments to enhance immune checkpoint blockade therapy

Zhi-Peng Peng,[1,2] Xing-Chen Liu,[1] Yong-Hao Ruan,[1] Da Jiang,[1] Ai-Qi Huang,[1] Wan-Ru Ning,[1] Ze-Zhou Jiang,[1] Limin Zheng ,[1,2] Yan Wu [1]

To cite: Peng Z-P, Liu X-C, Ruan Y-H, *et al*. Downregulation of phosphoserine phosphatase potentiates tumor immune environments to enhance immune checkpoint blockade therapy. *Journal for ImmunoTherapy of Cancer* 2023;**11**:e005986. doi:10.1136/jitc-2022-005986

► Additional supplemental material is published online only. To view, please visit the journal online (http://dx.doi.org/10.1136/jitc-2022-005986).

Z-PP and X-CL contributed equally.

Accepted 12 February 2023

[1]Guangdong Province Key Laboratory of Pharmaceutical Functional Genes, MOE Key Laboratory of Gene Function and Regulation, School of Life Sciences, Sun Yat-Sen University, Guangzhou, China
[2]State Key Laboratory of Oncology in Southern China, Collaborative Innovation Center for Cancer Medicine, Sun Yat-sen University Cancer Center, Guangzhou, China

Correspondence to
Dr Yan Wu;
wuyan32@mail.sysu.edu.cn

Professor Limin Zheng;
zhenglm@mail.sysu.edu.cn

ABSTRACT

Background Effects of immune checkpoint blockade (ICB) treatment in hepatocellular carcinoma (HCC) are limited. The current study explored the possibility of exploiting tumor metabolic switches to enhance HCC sensitivity to immune therapies.

Methods Levels of one-carbon (1C) metabolism and the expression of phosphoserine phosphatase (PSPH), an upstream enzyme of 1C pathway, were evaluated in paired non-tumor and tumor tissues from HCC. Underlying mechanisms mediating the role of PSPH in regulating the infiltration of monocytes/macrophages and $CD8^+$ T lymphocytes were studied through both in vitro and in vivo experiments.

Results PSPH was significantly upregulated in tumor tissues of HCC and its levels were positively correlated with disease progression. PSPH knockdown inhibited tumor growth in immunocompetent mice, but not in those with macrophage or T lymphocyte deficiencies, indicating the pro-tumor effects of PSPH were dependent on both immune components. Mechanistically, PSPH facilitated monocytes/macrophages infiltration by inducing the production of C-C motif chemokine 2 (CCL2), while at the same time reduced $CD8^+$ T lymphocytes recruitment through inhibiting the production of C-X-C Motif Chemokine 10 (CXCL10) in tumor necrosis factor alpha (TNF-α)-conditioned cancer cells. Glutathione and S-adenosyl-methionine were partially involved in regulating the production of CCL2 and CXCL10, respectively. sh*PSPH* (short hairpin RNA) transfection of cancer cells enhanced tumor sensitivity to anti-programmed cell death protein 1 (PD-1) therapy in vivo, and interestingly, metformin could inhibit PSPH expression in cancer cells and mimic the effects of sh*PSPH* in sensitizing tumors to anti-PD-1 treatment.

Conclusions By tilting the immune balance towards a tumor-friendly composition, PSPH might be useful both as a marker in stratifying patients for ICB therapy, and as an attractive therapeutic target in the treatment of human HCC.

WHAT IS ALREADY KNOWN ON THIS TOPIC

⇒ Immune checkpoint blockade (ICB) therapy has a low response rate in the treatment of hepatocellular carcinoma (HCC).

WHAT THIS STUDY ADDS

⇒ High expression of phosphoserine phosphatase (PSPH) promotes tumor immune escape by increasing the recruitment of monocytes/macrophages and reducing the infiltration of $CD8^+$ T lymphocytes, attenuating tumor response to immune checkpoint therapy.

HOW THIS STUDY MIGHT AFFECT RESEARCH, PRACTICE OR POLICY

⇒ PSPH might be useful both as a marker in stratifying patients for ICB therapy and as an attractive therapeutic target in the treatment of HCC.

INTRODUCTION

Folate metabolism, which supports a broad set of transformations known as one-carbon (1C) metabolism, is a universal metabolic process that serves to activate and transfer 1C units for biosynthetic processes.[1–3] Its products include purine, thymidine, methionine, nicotinamide adenine dinucleotide phosphate (NADPH), and so on, and primarily impact DNA synthesis, epigenetics and mitochondrial redox homeostasis.[4–8] 1C metabolism has been found upregulated in many tumors and targeting 1C metabolism has led to the first selective chemotherapeutic agents (methotrexate) in the treatment of leukemias.[9–11] New genomics and metabolomics approaches have highlighted distinctive aspects of 1C metabolism in cancer and rekindled interest in targeting this pathway with more selective modulators. However, studies about tumor 1C metabolism have been largely focused on cancer cells, with its possible impact on or interaction with tumor immune environments largely unknown. Moreover, given the complexity of 1C metabolism, the lack of an effective single target for 1C metabolism intervention and the limited

inhibitors or modulators currently available for selectively targeting 1C enzymes or their products also add to the difficulties of exploiting this pathway for clinical use.

Immune microenvironments influence and determine the clinical outcome and therapeutic responsiveness to immune checkpoint blockade (ICB) treatment of patients with cancer, and a 'cold' tumor microenvironment (particularly low effective T cell infiltration due to physical barrier or an imbalance of respective chemokines, such as high myeloid-related C-C motif chemokine 2 (CCL2) and low CD8-related C-X-C Motif Chemokine 9 (CXCL9) and C-X-C Motif Chemokine 10 (CXCL10) levels) has been indicated as an important biomarker for resistance to ICB treatment for some tumors.[12–17] However, mechanisms involved in regulating the balance of specific chemokine productions in tumor environments have not been fully understood. Deciphering mechanisms governing chemokines balance might assist physicians in distinguishing patients who are most likely to benefit from ICB therapy.

In the current study, we aimed to figure out possible changes in 1C metabolism in human hepatocellular carcinoma (HCC), its relationship with tumor immune environments and how their possible interaction might influence the responsiveness of tumor to ICB therapeutics. Our results showed that an upstream 1C pathway enzyme, namely phosphoserine phosphatase (PSPH), was significantly upregulated in tumor than non-tumor liver tissues of human HCC, and its level exhibited a positive correlation with disease progression. While it did not show direct effects on the physiology of cancer cells themselves, PSPH in cancer cells could induce monocytes/macrophages infiltration and reduce $CD8^+$ T cells recruitment into the tumor milieu through increasing CCL2 expression and suppressing CXCL10 production, respectively. PSPH knockdown, alone or in combination with ICB agents, could significantly reduce tumor progression in mice in vivo. Therefore, PSPH might represent itself as both a possible diagnostic landmark and a candidate for immune-based cancer therapies for patients with HCC.

MATERIALS AND METHODS

Human HCC tissue samples

Liver tissue samples were obtained from 351 untreated patients with pathologically confirmed HCC at Sun Yat-sen University Cancer Center and Sun Yat-sen Memorial Hospital between 2006 and 2020. Patients with concurrent autoimmune disease, HIV, or syphilis were excluded. Among these patients, 321 (cohort 1) who had clinical biochemistry test results and follow-up data were used for immunohistochemical staining and subsequent correlations and overall survival (OS) analysis. Another 30 fresh liver tissues (cohort 2) were used for RNA, protein, and metabolites-related experiments. Non-tumor sites were defined as areas at least 3 cm away from tumor sites. The clinical characteristics of all patients are summarized in online supplemental table S1.

Animals

Wild-type male C57BL/6 mice and Balb/c nude mice were purchased from Guangdong Medical Laboratory Animal Center (Guangzhou, China), and NOD-$Prkdc^{em26Cd52}Il2rg^{em26Cd22}$ mice (NCG) mice were purchased from GemPharmatech (Nanjing, China). All mice were maintained under specific pathogen-free conditions and were used between 6 weeks and 8 weeks of age. Mice were also euthanized when they experienced open skin lesions, weight loss >15% total body weight, or failed to thrive.

Mouse tumor models and treatments

Subcutaneous tumor model: A total of 8×10^5 Hepa1-6, sh*PSPH*-Hepa1-6, and sh*PLKO*-Hepa1-6 cells were subcutaneously transplanted into the flanks of mice. Mice were monitored for tumor growth every 3 days. Tumor size was measured by use of a caliper and calculated using the formula Volume = (length) $(width)^2/2$. The endpoint was defined as the time at which a progressively growing tumor reached 2000 mm^3 in volume.

Orthotopic hepatic tumor model: A total of 8×10^5 tumor cells were suspended in 25 µl of 50% basement membrane extract (3432-005-01, Trevigen), and intrahepatically injected into the left lobe of the liver of anesthetized 6-week-old C57BL/6 mice. Mice bearing luciferase-expressing Hepa1-6 tumors were intraperitoneally injected with 1.5 mg D-luciferin (2779, Biovision) to monitor orthotopic tumor growth with a Xenogen in vivo imaging system (PerkinElmer).

In some experiments, 10 mg/kg $GdCl_3$ (4399770, Sigma-Aldrich) was administered intraperitoneally every 3 days beginning on day 0 to deplete monocytes and macrophages. In some experiments, Rat IgG2a isotype control antibody (BP0089, Bioxcell), or 100 µg of antimouse CD8a antibody (BE0004, Bioxcell) were intraperitoneally injected beginning on day 6, and tumor infiltrated $Ly6C^+$ monocytes and $F4/80^+$ macrophages were intratumorally injected beginning on day 6. In other experiments, Rat IgG2a isotype control antibody, 50 µg of antimouse programmed cell death protein 1 (PD-1) antibody (BE0146, Bioxcell), 2 mg metformin (HY-17471A, MedChemExpress), or 2 mg metformin in combination with antimouse PD-1 antibody were intraperitoneally injected beginning on day 6 or day 9 (metformin: every day; antibodies: every 3 days).

Statistical analysis

Statistical tests used are indicated in the figure legends. Data were tested for normality using Shapiro–Wilk test or Kolmogorov-Smirnov test and variance homogeneity using F-test. Correlations between parameters were measured by Pearson correlation. Survival curves were calculated by the Kaplan-Meier method and analyzed by the log-rank test. The Cox proportional hazards model was used to identify prognostic factors through univariate and multivariate analyses. For comparing normally distributed continuous variables that were homogeneity

of variance, we used a two-tailed Student's t-test or two-way analysis of variance with Bonferroni's multiple comparisons test, respectively. For comparing normally distributed continuous variables that were heterogeneity of variance, we used Welch's t-test. The results are expressed as the means±SEMs. Statistical analysis was performed with GraphPad Prism V.9 (GraphPad Software, La Jolla, California, USA). The following are the thresholds for statistical significance: *p<0.05; **p<0.01; and ***p<0.001; ns, no significance.

Further details of materials and methods are provided in the online supplemental materials.

RESULTS

1C metabolism is upregulated in human HCC and levels of PSPH expression are positively correlated with disease progression

Transcriptome data from The Cancer Genome Atlas and fresh HCC tissues (50 and 5 patients, respectively, with paired tumor and non-tumor data) showed that levels of 1C metabolic enzymes expression were significantly different between tumor and paired non-tumor liver tissues, with *PSPH, methionine adenosyltransferase 2A (MAT2A), methylenetetrahydrofolate dehydrogenase 1 like (MTHFD1L), aldehyde dehydrogenase 1 family member L2 (ALDH1L2), serine hydroxymethyltransferase 2 (SHMT2), phosphoglycerate dehydrogenase (PHGDH)* increased, and aldehyde dehydrogenase 1 family member L1 (*ALDH1L1), methionine adenosyltransferase 1A (MAT1A)* decreased in tumors (figure 1A–C). Western blotting confirmed the difference in PSPH, MAT2A, MTHFD1L, ALDH1L2, ALDH1L1 and MAT1A expression between paired tumor and non-tumor tissues (figure 1D and online supplemental figure S1A, n=3). Consistently, intermediate metabolites from the main 1C pathway—3-phosphoserine (3PSer), serine, and methionine—were higher, while glycine from the branch 1C pathway was lower in tumor than paired non-tumor tissues (figure 1E,F, n=5).

PSPH was the most significantly changed 1C enzyme in HCC tumors. While exhibiting very low levels of expression in non-tumor liver tissues, PSPH was increased in tumors as validated through quantitative PCR (Q-PCR), western blotting, and immunohistochemistry (IHC) staining analysis (figure 1G–I, n=17 for Q-PCR, n=7 for western blotting and IHC). When patients with HCC who had received curative resection with follow-up data were divided into two groups according to the median value of their PSPH expression level in tumor tissues, as shown in figure 1J, PSPH expression was found negatively associated with the OS of patients with HCC ($PSPH^{high}$: n=160, $PSPH^{low}$: n=161, p=0.001). Moreover, levels of PSPH expression in tumor tissues were positively associated with aspartate aminotransferase/alanine aminotransferase (AST/ALT), P^+, and lactate dehydrogenase (LDH) levels in the peripheral blood of paired patients with HCC (online supplemental figure S2), and could serve as an independent prognostic factor for the OS of patients with HCC (p=0.027, online supplemental table S2). These results suggested that 1C metabolism was switched on in human HCC tissues, and its key enzyme—PSPH—might be upregulated to facilitate disease progression.

PSPH orchestrates macrophages and $CD8^+$ T cells accumulation in tumor microenvironments and promotes tumor growth in mice in vivo

To understand the protumor effects of PSPH, two sh*PSPH* RNA sequences (designated as sh*PSPH1* and sh*PSPH2*) were designed to transfect Hepa1-6 tumor cells. While neither sh*PSPH* RNA impacted tumor cell viability and apoptosis in vitro, they could both significantly inhibit tumor growth in immunocompetent C57BL/6 mice in vivo compared with the sh*PLKO* control (empty cloning vector) (online supplemental figure S3, n=4 and figure 2A, n=5). In contrast, no significant difference in terms of tumor growth was displayed between the sh*PSPH*-Hepa1-6 and sh*PLKO*-Hepa1-6 tumors when they were transplanted into the NCG mice (figure 2B, n=6), and only a modest difference was observed in monocytes/macrophages-depleted mice (figure 2C, n=3), or Balb/c nude mice (figure 2D, n=3), suggesting that the pro-tumor effects of PSPH might be mediated through both macrophages and T lymphocytes. Supporting this hypothesis, replenishment of tumor-associated monocytes and macrophages, or depletion of $CD8^+$ T cells, or a combination of tumor-associated monocytes and macrophages replenishment with $CD8^+$ T cells depletion could effectively relieve the attenuated tumor growth of sh*PSPH*-Hepa1-6 cells in comparison to the sh*PLKO* control in C57BL/6 mice in vivo (online supplemental figure S4, n=4).

To explore how PSPH-depleted cancer cells might impact immune components, mRNA array was performed to compare genes differently expressed between sh*PSPH* and sh*PLKO* hepatoma cells (PLC/PRF/5 and SNU449 cells; online supplemental figure S5A). Of the enriched pathways, immune cell chemotaxis-related genes, such as *CCL2* and *CXCL10*, were substantially downregulated or upregulated in sh*PSPH* cells compared with the sh*PLKO* controls, while major histocompatibility complex (MHC) class genes, such as *humanleukocyteantigen A (HLA-A)* and *humanleukocyteantigen B (HLA-B)*, were markedly increased (online supplemental figure S5B,C), implicating PSPH might impact immune infiltration, as well as T cell activation through chemokines and MHC-related pathways. To test the chemokine hypothesis, we analyzed the levels of monocytes/macrophages-related CCL2 and $CD8^+$ T cells-related CXCL10 in our in vivo mice models. Results showed that levels of *CCL2* expression were significantly reduced while levels of *CXCL10* were markedly increased in sh*PSPH*-transfected Hepa1-6 tumors than in the sh*PLKO* controls in C57BL/6 mice (figure 2E, n=5). Accordingly, when measured by flow cytometry, levels of monocytes ($Ly6C^+$ cells) and macrophages ($F4/80^+$ cells) infiltration were reduced in both sh*PSPH1*-transfected and sh*PSPH2*-transfected tumors, while levels of $CD8^+$

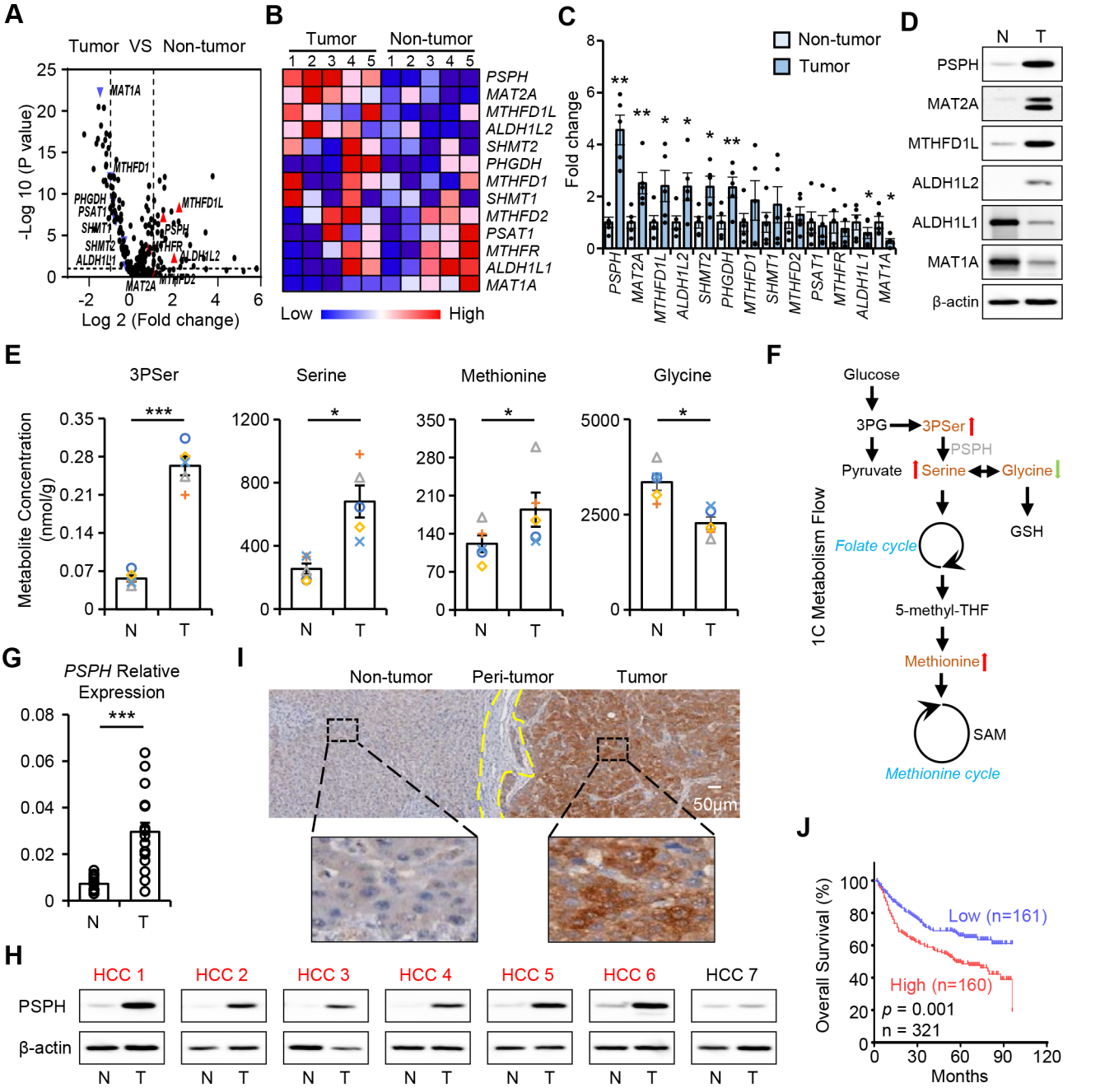

Figure 1 One-carbon (1C) metabolism is upregulated in human hepatocellular carcinoma (HCC) and levels of phosphoserine phosphatase (PSPH) expression are positively correlated with disease progression. (A–C) Transcriptome data from The Cancer Genome Atlas (n=50, (A)) and fresh HCC tissues (n=5, (B–C)). (D) 1C enzymes in fresh HCC tissues were determined by western blotting (n=3; N: non-tumor; T: tumor). (E–F) Key 1C metabolites in fresh HCC tissues were analyzed by mass spectrometry (n=5; N: non-tumor; T: tumor). (G–I) PSPH expression in fresh HCC tissues were determined by quantitative PCR (Q-PCR) (n=17, (G)), western blotting (n=7, (H)) and IHC staining (n=7, (I)) (N: non-tumor; T: tumor). (J) Overall survival of patients with HCC with high or low tumor expression of PSPH. Data are mean±SEM. Statistical methods: paired t-test (A, C, E), Welch's t-test (G), Kaplan-Meier method and log-rank test (J). *p<0.05, **p<0.01, ***p<0.001. 3PG, 3-phosphoglycerate; GSH, glutathione; SAM, S-adenosyl-methionine.

T cells infiltration were significantly increased in those PSPH-depleted tumors compared with their sh*PLKO* controls (figure 2F, n=5). The reduced accumulation of monocytes (Ly6C$^+$ cells) and macrophages (F4/80$^+$ cells), and increased infiltration of CD8$^+$ T cells in PSPH-depleted tumors compared with sh*PLKO* controls were further confirmed through immunofluorescent staining of tumor sections (figure 2G,H, n=5). Therefore, the above data implied that PSPH expression in tumor cells might facilitate tumor progression through both increasing the CCL2-mediated monocytes/macrophages accumulation and reducing the CXCL10-mediated CD8$^+$ T cells infiltration.

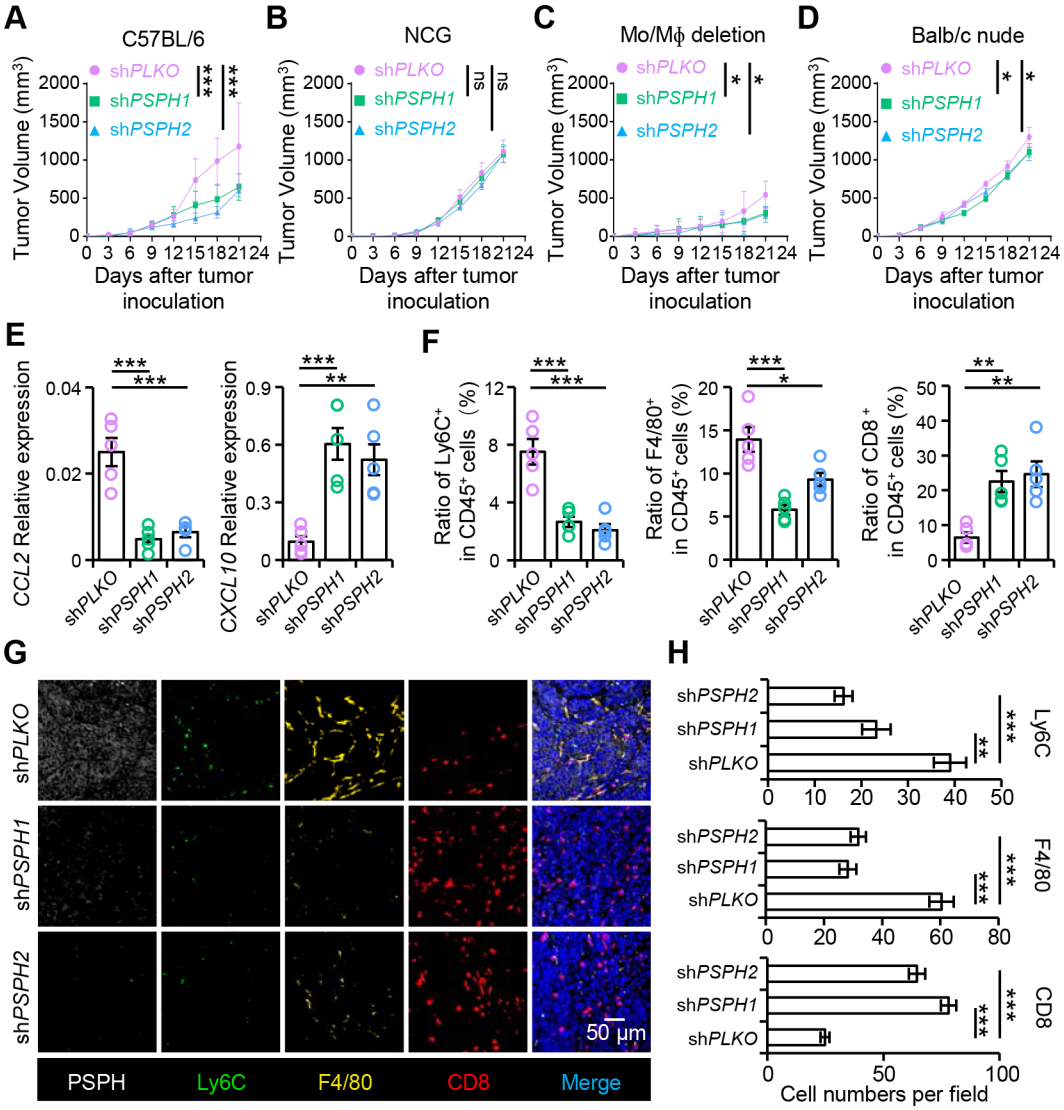

Figure 2 Phosphoserine phosphatase (PSPH) orchestrates macrophages and CD8$^+$ T cells accumulation in tumor microenvironments and promotes tumor growth in mice in vivo. (A–D) Tumor growth of sh*PLKO*-transfected or sh*PSPH*-transfected Hepa1-6 cells in C57BL/6 mice (n=5, (A)), NCG (NOD-Prkdc^{em26Cd52}Il2rg^{em26Cd22}) mice (n=6, (B)), monocytes/macrophages-depleted mice (n=3, (C)), or Balb/c nude mice (n=3, (D)). (E)Quantitative PCR (Q-PCR) showed the levels of *CCL2* and *CXCL10* in sh*PLKO*-transfected or sh*PSPH*-transfected Hepa1-6 tumors in C57BL/6 mice (n=5). (F–H) Flow cytometry (F) and immunofluorescent analysis (G–H) showed the levels of Ly6C$^+$ monocytes, F4/80$^+$ macrophages, and CD8$^+$ T cells infiltration in sh*PLKO*-transfected or sh*PSPH*-transfected Hepa1-6 tumors in C57BL/6 mice (n=5). Data are mean±SEM. Statistical methods: Two-way analysis of variance with Bonferroni's multiple comparisons test (A, B, C, D), Student's t-test (E, F, H). *p<0.05, **p<0.01, ***p<0.001; ns, no significance.

PSPH regulates tumor release of CXCL10 and CCL2 through the S-adenosyl-methionine and glutathione pathways, respectively

To explore mechanisms mediating the tumor release of CCL2 and CXCL10, hepatoma cell lines PLC/PRF/5 and SNU449, which exhibited high basal levels of PSPH expression, were employed in the in vitro experimental models. Interestingly, both PLC/PRF/5 and SNU449 cells expressed very low levels of CCL2 and CXCL10 unless they were stimulated with a low dose of TNF-α. Effects of other cytokines were relatively minor in terms of inducing CCL2 and CXCL10 expression in these cells (online supplemental figure S6A,B, n=3). Since low levels of TNF-α were prevalent in tumor microenvironments and might be further elevated on various immune therapies, and given that sh*PSPH1* and sh*PSPH2* could reduce CCL2 expression while increasing CXCL10 expression compared with sh*PLKO* controls in TNF-α-exposed PLC/PRF/5 and SNU449 cells (figure 3A and online supplemental figure S7A, n=5), we considered this a clinically relevant model to conduct the mechanistic experiments.

It has been reported that CXCL10 expression was negatively regulated by H3K27me3,[18] whose methylation depended on the methyl groups provided by S-adenosyl-methionine (SAM) downstream of 1C metabolism. Therefore, we first evaluated whether PSPH regulated

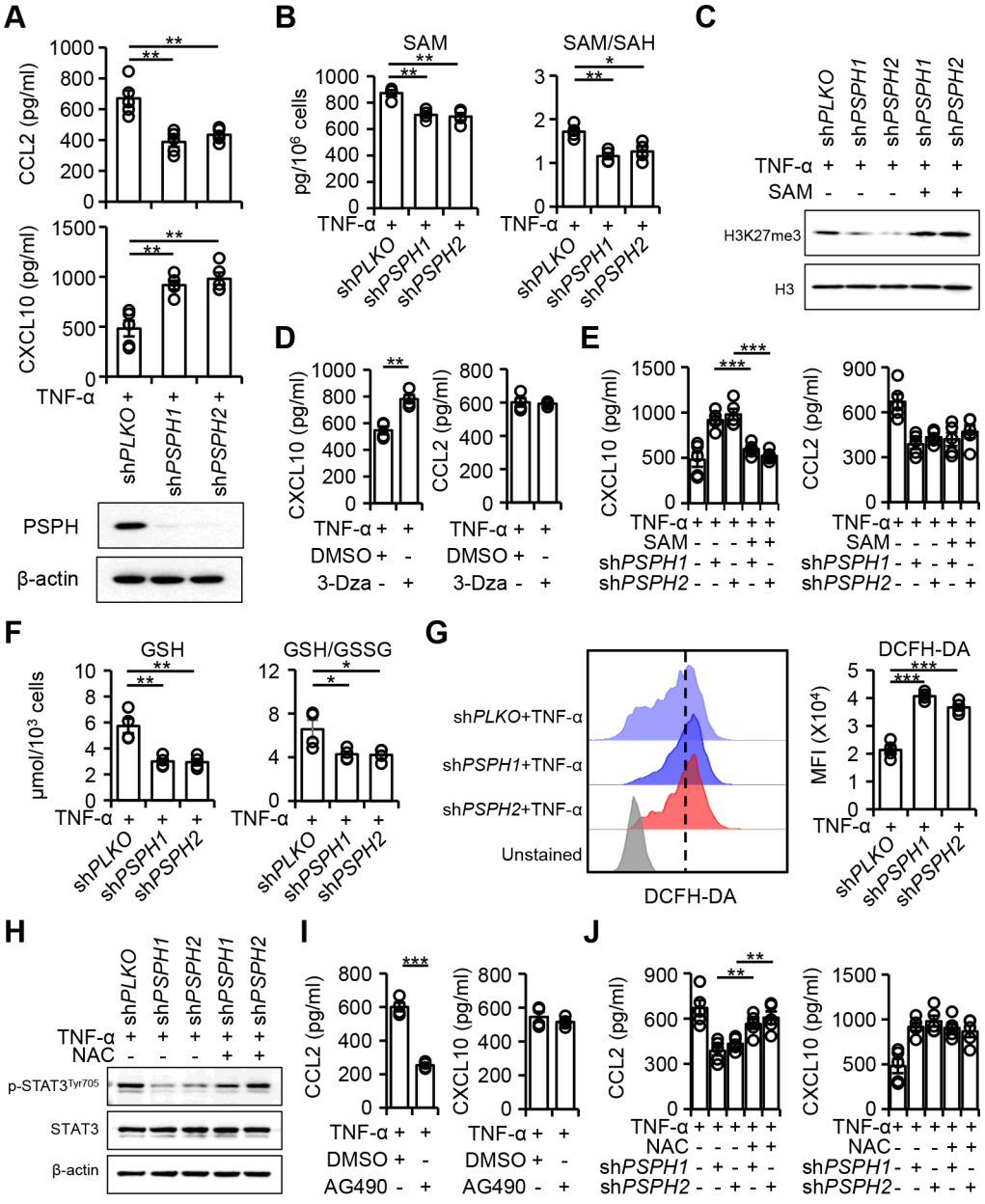

Figure 3 Phosphoserine phosphatase (PSPH) regulates tumor release of CXCL10 and CCL2 through the S-adenosyl-methionine (SAM) and glutathione (GSH) pathways, respectively. PLC/PRF/5 cells were left untreated or transfected with sh*PLKO* or sh*PSPH*, and treated with TNF-α. (A) Western blotting showed PSPH, and ELISA showed CCL2, CXCL10 levels in sh*PLKO* or sh*PSPH* tumor cells (n=5). (B) SAM and SAM/SAH were measured in sh*PLKO* or sh*PSPH* tumor cells (n=4). (C) Western blotting showed H3K27me3 in sh*PLKO* or sh*PSPH* tumor cells, in the presence or absence of supplemented SAM (n=3). (D–E) ELISA showed CCL2 and CXCL10 levels in 3-Deazaadenosine hydrochloride (3-Dza)-treated or 3-Dza-untreated tumor cells (n=4, (D)), or in sh*PLKO* or sh*PSPH* transfected tumor cells, in the presence or absence of supplemented SAM (n=5, (E)).(F) GSH and GSH/GSSG were measured in sh*PLKO* or sh*PSPH* tumor cells (n=4). (G) Flow cytometry analysis showed ROS levels in sh*PLKO* or sh*PSPH* tumor cells (n=4). (H) Western blotting showed p-STAT3^{Tyr705}, STAT3 in sh*PLKO* or sh*PSPH* tumor cells, in the presence or absence of supplemented NAC (n=3). (I–J) ELISA showed CCL2 and CXCL10 levels in AG490-treated or AG490-untreated tumor cells (n=4, (I)), or in sh*PLKO* or sh*PSPH* transfected tumor cells, in the presence or absence of supplemented NAC (n=5, (J)). Data are mean±SEM. Statistical methods: Student's t-test (A, B, D, E, F, G, I, J). *p<0.05, **p<0.01, ***p<0.001. SAM, S-adenosyl-methionine (SAM); SAH, S-adenosyl-homocysteine; GSH, glutathione; GSSG, oxidized glutathione; DMSO, dimethyl sulfoxide.

CXCL10 expression through this pathway. As shown in figure 3B,C, online supplemental figures S1B and S7B,C (n=4 for B, n=3 for C), levels of SAM, SAM/SAH, and H3K27me3 were all significantly reduced in sh*PSPH*-transfected PLC/PRF/5 and SNU449 cells compared with their respective sh*PLKO* counterparts. Notably, 3-Deazaadenosine hydrochloride (3-Dza), an inhibitor decreasing SAM:SAH ratio and suppressing SAM-dependent methylation reactions, could mimic the effects of sh*PSPH* transfection in increasing CXCL10 expression

in TNF-α-exposed wild-type PLC/PRF/5 and SNU449 cells, while leaving the expression of CCL2 in these cells unimpacted (figure 3D and online supplemental figure S7D, n=4). On the flip side, the addition of SAM could attenuate the increase of CXCL10 expression in sh*PSPH*-transfected PLC/PRF/5 and SNU449 cells compared with their sh*PLKO* controls, while did not impact the expression of CCL2 (figure 3E and online supplemental figure S7E, n=5). Interestingly, sh*PSPH* also increased levels of *HLA-A* and *HLA-B* expression in PLC/PRF/5 and SNU449 cells compared with sh*PLKO* controls (online supplemental figure S8A, n=3). While 3-Dza could mimic the effects of sh*PSPH* transfection in increasing both the *HLA-A* and *HLA-B* expression in wild-type PLC/PRF/5 and SNU449 cells, the addition of SAM could attenuate the increase of *HLA-A* and *HLA-B* expression in sh*PSPH*-transfected PLC/PRF/5 and SNU449 cells compared with their sh*PLKO* controls (online supplemental figure S8A,B, n=3). These data suggested that PSPH-mediated high levels of SAM and H3K27me3 might inhibit the expression of CXCL10 and HLA-A/B by hepatoma cells, and depletion of PSPH could release the production or expression of these molecules.

Glutathione (GSH) is another essential downstream metabolite of the 1C pathway that can interact with reactive oxygen species (ROS) to regulate cellular redox balance.[19] As shown in figure 3F,G and online supplemental figure S7F,G (n=4), sh*PSPH*-transfected PLC/PRF/5 and SNU449 cells reduced GSH level and GSH/GSSG ratio, while increasing the ROS level in comparison to their sh*PLKO* counterparts. Given that ROS could regulate several signaling pathways and their respective downstream functions, we tried to explore which pathway might be impacted by sh*PSPH* transfection and possibly mediate CCL2 expression by hepatoma cells. Gene enrichment analysis of the transcriptome profiles of sh*PSPH*-transfected hepatoma cells or sh*PLKO*-transfected control cells showed that the Janus kinase-signal transducer and activator of transcription (JAK-STAT) signaling pathway was preferentially inhibited in sh*PSPH*-transfected hepatoma cells (p=0.049 for PLC/PRF/5 and p=0.010 for SNU449), with other signaling pathways such as TNF-α, mitogen-activated protein kinase (MAPK), and phosphoinositide 3-kinase-protein kinase B (PI3K-AKT) largely unimpacted (online supplemental figure S9, n=2). Interestingly, the protein levels of Phospho-Stat3 (Ser705) (p-STAT3^{Tyr705}), but not other STAT family members, were significantly downregulated in sh*PSPH*-transfected PLC/PRF/5 and SNU449 cells compared with sh*PLKO* controls (figure 3H, online supplemental figures S1C and S7H, n=3 and data not shown). Importantly, N-Acetyl-L-cysteine (NAC, a ROS scavenger) could antagonize the effects of sh*PSPH* to re-induce the expression of p-STAT3^{Tyr705} in sh*PSPH*-transfected PLC/PRF/5 and SNU449 cells (figure 3H and online supplemental figure S7H, n=3), implying that the effect of PSPH on signal transducer and activator of transcription 3 (STAT3) activation was mainly mediated through ROS. When chemokines were measured, AG-490, a STAT3 signaling inhibitor, could mimic the effects of sh*PSPH* in reducing the production of CCL2 in wild-type PLC/PRF/5 and SNU449 cells, while leaving those of CXCL10 unimpacted (figure 3I and online supplemental figure S7I, n=4), and NAC, which re-induced p-STAT3^{Tyr705} in sh*PSPH*-transfected hepatoma cells, could abrogate the sh*PSPH*-induced inhibition of CCL2 production in these cells compared with their sh*PLKO* controls, while it did not impact the expression of CXCL10 (figure 3J and online supplemental figure S7J, n=5). Together, these data indicated that PSPH-mediated ROS scavenging by GSH might induce CCL2 production in hepatoma cells through the activation of the STAT3 signaling pathway.

We also compared the difference between TNF-α-untreated and TNF-α-treated hepatoma cells in terms of their levels of the above-mentioned pathways. As shown in online supplemental figure S6C,D, TNF-α did not impact ratios of SAM/SAH, but could decrease levels of H3K27me3 in cancer cells, which explained its effects in modestly inducing CXCL10 production by these cells (online supplemental figure S6A). TNF-α did not impact levels of GSH/GSSG and ROS expression in cancer cells (online supplemental figure S6E,F), and the basal levels of p-STAT3^{Tyr705} in untreated cells were relatively low (online supplemental figure S6G), possibly due to a lack of stimulation. When cells were stimulated with TNF-α, they substantially increased levels of p-STAT3^{Tyr705} (online supplemental figure S6G) and thus upregulated the production of CCL2 (online supplemental figure S6B). The TNF-α-induced upregulation of CXCL10 and CCL2 could be significantly enhanced or abrogated by treating these cells with sh*PSPH* (figure 3A).

Correlations between the PSPH level, p-STAT3/H3K27me3 level, CCL2/CXCL10 expression, and macrophages/effector T cells infiltration in human HCC samples

To confirm the above findings concerning mechanisms regulating CCL2 and CXCL10 expression by PSPH, serial sections from 20 patients with HCC were stained with different markers. As shown in figure 4A–C, levels of PSPH were found positively associated with those of p-STAT3, *CCL2*, and CD68$^+$ cells infiltration in tumor tissues of HCC (PSPH and p-STAT3: r=0.6202, p=0.0035; PSPH and *CCL2*: r=0.7217, p=0.0003; PSPH and CD68$^+$ cells: r=0.6963, p=0.0006), and while they were positively associated with levels of H3K27me3 expression (r=0.6555, p=0.0017), levels of PSPH were negatively correlated with those of *CXCL10* and CD8$^+$ T cells infiltration in HCC tumors (PSPH and *CXCL10*: r=−0.6206, p=0.0035; PSPH and CD8$^+$ T cells: r=−0.6205, p=0.0035). Consistently, levels of p-STAT3 expression were positively correlated with *CCL2* expression and CD68$^+$ cells infiltration (figure 4A,D; p-STAT3 and *CCL2*: r=0.7493, p=0.0001; p-STAT3 and CD68$^+$ cells: r=0.6507, p=0.0019), while levels of H3K27me3 expression were negatively associated with *CXCL10* expression and CD8$^+$ T cells

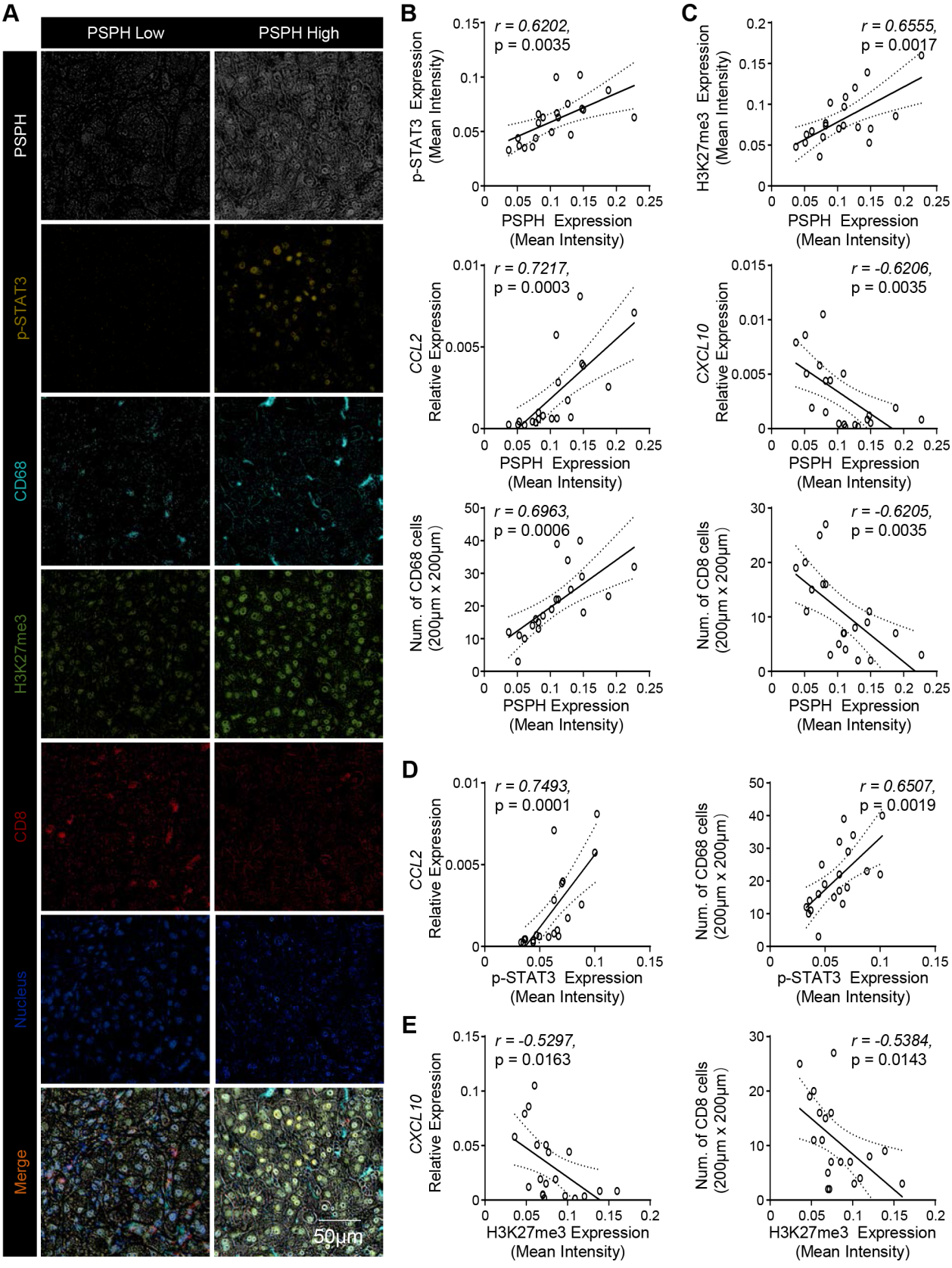

Figure 4 Correlations between the phosphoserine phosphatase (PSPH) level, p-STAT3/H3K27me3 level, *CCL2*/*CXCL10* expression, and macrophages/effector T cells infiltration in human hepatocellular carcinoma (HCC) samples. (A) Immunofluorescent analysis showed the expression of indicated markers in HCC tumor sections with low or high levels of PSPH. (B–E), Correlation between the levels of PSPH expression, p-STAT3 expression, H3K27me3 expression, *CCL2* mRNA, *CXCL10* mRNA, $CD68^+$ cells infiltration, and $CD8^+$ T cells infiltration in HCC tumor samples were analyzed by quantitative PCR (Q-PCR) or IHC. n=20. Statistical methods: Pearson correlation and linear regression analysis (B, C, D, E).

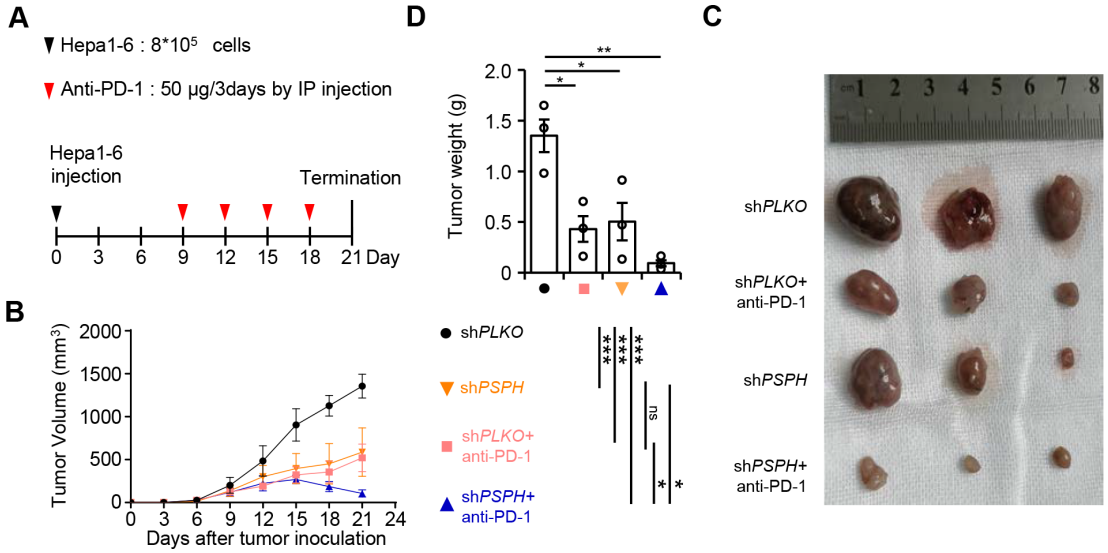

Figure 5 sh*PSPH* sensitizes hepatoma to anti-PD-1 antibody treatment in subcutaneous mice model. (A) C57BL/6 mice with established sh*PLKO*-transfected or sh*PSPH* -transfected Hepa1-6 tumors were intraperitoneally injected with or without anti-PD-1 antibodies at indicated times. (B–D) Tumor growth (B, C) (day 21), and tumor weight (D) (day 21) were monitored. n=3. Data are mean±SEM. Statistical methods: Two-way analysis of variance with Bonferroni's multiple comparisons test (B), Student's t test (D). *p<0.05, **p<0.01, ***p<0.001; ns, no significance. IP,intraperitoneally injected.

infiltration in tumors of HCC (figure 4A,E; H3K27me3 and *CXCL10*: r=−0.5297, p=0.0163; H3K27me3 and $CD8^+$ T cells: r=−0.5384, p=0.0143).

sh*PSPH* sensitizes hepatoma to anti-PD-1 antibody treatment in mice in vivo

Tipping the scale towards a quantitatively and qualitatively immune-effective microenvironment is essential to T cell-related immunotherapies. We went on to establish whether the depletion of PSPH expression could synergistically act with ICB therapeutics to inhibit tumor progression of HCC. Wild-type C57BL/6 mice were subcutaneously inoculated with sh*PLKO*-Hepa1-6 cells or sh*PSPH*-Hepa1-6 cells, before being treated with or without anti-PD-1 antibodies (figure 5A). As shown in figure 5B–D (n=3), tumor growth was inhibited in the sh*PSPH*-transfected group, or the sh*PLKO*-transfected tumor treated with anti-PD-1, in comparison to the sh*PLKO* control in terms of both tumor volume and tumor weight. Importantly, the combination of PSPH depletion with anti-PD-1 was more effective in prohibiting tumor growth than either treatment alone, indicating a synergistic effect between these two therapeutic treatments.

Orthotopic Hepa1-6 hepatoma mice model was also established to confirm the above observations. Wild-type C57BL/6 mice with orthotopic sh*PLKO*-Hepa1-6 or sh*PSPH*-Hepa1-6 hepatomas were treated with or without anti-PD-1 antibodies (figure 6A). As shown in figure 6B–E (n=3), sh*PSPH*-Hepa1-6 hepatomas showed reduced *CCL2* expression, increased *CXCL10* production, reduced $Ly6C^+$ cells and $F4/80^+$ cells infiltration, and increased $CD8^+$ T cells accumulation in comparison to their respective sh*PLKO* controls. Similar to those observed in subcutaneous mice models, tumor growth was inhibited in the sh*PSPH* transfected group, or the sh*PLKO*-transfected tumor treated with anti-PD-1 antibodies compared with the sh*PLKO* control, while the combination of PSPH depletion with anti-PD-1 was more effective in prohibiting tumor growth than either treatment alone (figure 6F,G), confirming a synergistic effect between these two therapeutic treatments.

Moreover, our results also showed that $CD8^+$ T cells purified from sh*PSPH*-Hepa1-6 tumors (both subcutaneous and orthotopic) exhibited higher expression of Granzyme B and perforin in comparison to their sh*PLKO*-tumor derived counterparts—although at levels much lower than those purified from tumors treated with anti-PD-1 antibodies (online supplemental figure S10, n=3)—an effect which might be explained by the higher expression of *HLA-A* and *HLA-B* molecules by sh*PSPH* tumor cells as observed in in vitro experiments (online supplemental figure S8A,B, n= 3).

Metformin mimics the effects of sh*PSPH* in regulating chemokines production, immune composition, and hepatoma growth in mice in vivo

Given that no PSPH inhibitor is currently available and metformin, an antidiabetes and an antiaging chemical, has been implicated to be able to modulate tumor metabolism,[20–22] we tried to explore whether metformin might impact PSPH expression and thus influence HCC tumor progression. First, our results showed that metformin did not directly impact the viability and apoptosis of Hepa1-6 cells in vitro (online supplemental figure S11A,B, n=4), but could reduce levels of PSPH expression in Hepa1-6 tumors in C57BL/6 mice in vivo (figure 7A, n=4), while leaving other major enzymes of the 1C pathway, such as MTHFD1L, ALDH1L2, and MAT2A largely unimpacted (figure 7A, online supplemental figure S11C, n=4). Meanwhile, metformin could reduce *CCL2* expression,

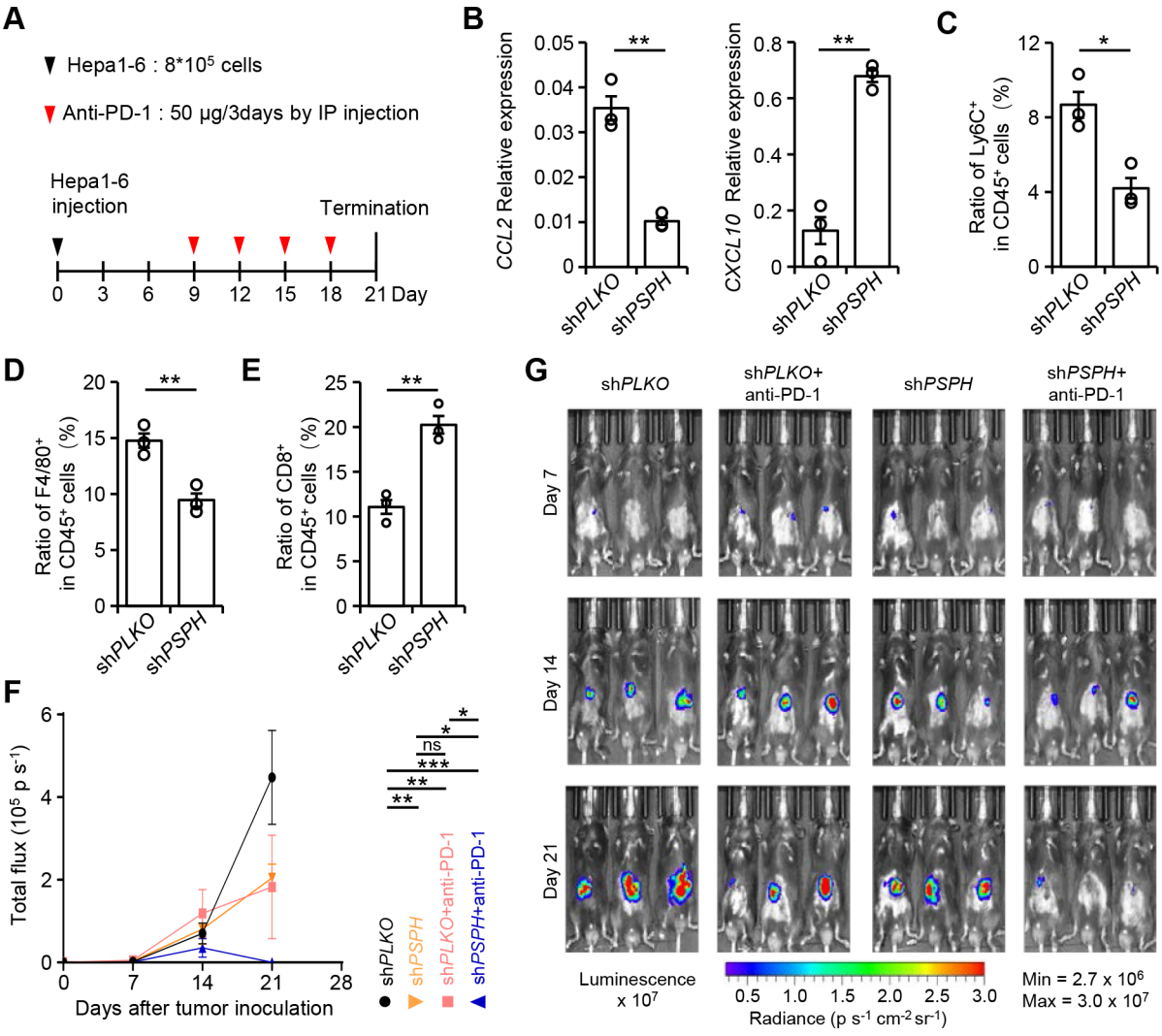

Figure 6 sh*PSPH* sensitizes hepatoma to anti-PD-1 antibody treatment in orthotopic mice model. (A) C57BL/6 mice with established orthotopic sh*PLKO*-transfected or sh*PSPH*-transfected, luminescence-positive, Hepa1-6 tumors were intraperitoneally injected with or without anti-PD-1 antibodies at indicated times. (B–E) *CCL2* and *CXCL10* levels (n=3, (B)), Ly6C$^+$ monocytes, F4/80$^+$ macrophages, and CD8$^+$ T cells infiltrations (n=3, (C–E)) in tumors were determined by quantitative PCR (Q-PCR), and flow cytometry, respectively. (F–G) Real-time tumor growth was monitored. n=3. Data are mean±SEM. Statistical methods: Two-way analysis of variance with Bonferroni's multiple comparisons test (F), Student's t-test (B, C, D, E). *p<0.05, **p<0.01, ***p<0.001; ns, no significance. IP, intraperitoneally injected.

increase *CXCL10* production, reduce Ly6C$^+$ cells and F4/80$^+$ cells infiltration, and increase CD8$^+$ T cells accumulation in tumor tissues compared with their respective control treatment groups, which mirrored the effects of sh*PSPH* transfection of Hepa1-6 tumors (figure 7B–E, online supplemental figure S11D, n=3). Notably, while anti-PD-1 or metformin treatment could inhibit tumor growth both in size and weight compared with the non-treated control in C57BL/6 mice, anti-PD-1 combined with metformin could reduce tumor growth more effectively than either treatment alone (figure 7F–H, n=3), an effect also similar to that observed from anti-PD-1 together with PSPH depletion.

DISCUSSION

The ever-changing immune components—in particular, the intrinsic or developed myeloid-cell-rich and effector-T cell-low tumor microenvironment—poses unique challenges for patients with cancer to mount effective responses to ICB therapy.[23–26] Unveiling the basic mechanisms determining the immune balance of tumor environments would facilitate the search for biomarkers that could predict clinical responses in different tumor types and for individual patients. Our current study provided evidence that PSPH from the 1C metabolic pathway might play an important yet unexpected role in determining the immune composition of tumor microenvironments of HCC. On cytokine stimulation, PSPH in cancer cells favored the infiltration of myeloid cells via the GSH-CCL2 axis, while prohibiting the infiltration of effector T cells via the SAM-CXCL10 pathway, thus tipping the

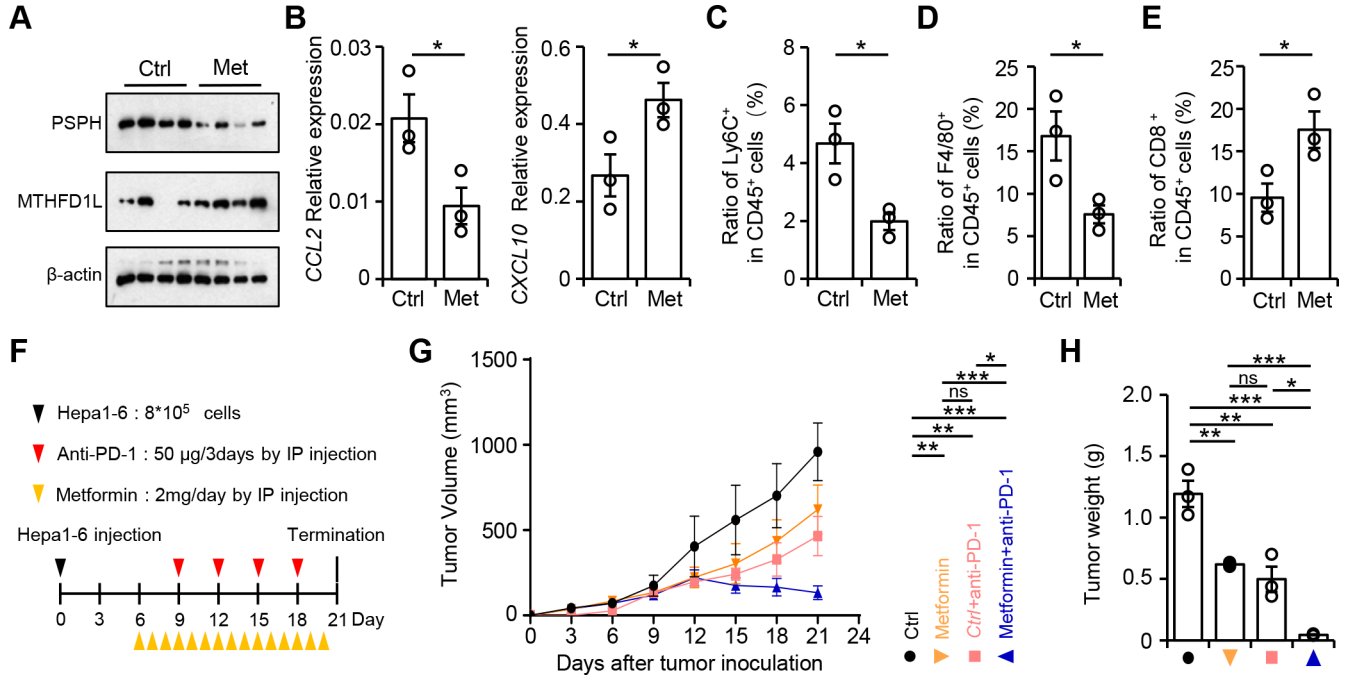

Figure 7 Metformin mimics the effects of sh*PSPH* in regulating chemokines production, immune composition, and hepatoma growth in mice in vivo. (A–E) Effects of Metformin (Met) on PSPH and MTHFD1L expression (n=4, (A)), *CCL2* and *CXCL10* levels (n=3, (B)), and Ly6C$^+$ monocytes, F4/80$^+$ macrophages, CD8$^+$ T cells infiltration (n=3, (C–E)) in Hepa1-6 tumors of C57BL/6 mice were determined by western blotting, quantitative PCR (Q-PCR), and flow cytometry, respectively. (F–H) C57BL/6 mice with established Hepa1-6 tumors were intraperitoneally injected with or without metformin, anti-PD-1 antibodies at indicated times (F), Tumor growth (n=3 for (G), n=3 for (H) (day 21)) was monitored. Ctrl: PBS. Data are mean±SEM Statistical methods: Student's t-test (B, C, D, E, H), Two-way analysis of variance with Bonferroni's multiple comparisons test (G). *p<0.05, **p<0.01, ***p<0.001; ns, no significance. IP, intraperitoneally injected; PBS, phosphate buffer saline.

scale towards immunosuppression and attenuating tumor responses to ICB therapies.

Tumor microenvironments are heterogeneous in terms of both cell composition and nutrient availability, and some metabolic shifts observed in cancer cells might not be unique to the tumor milieus.[27–29] Therefore, the prospect of targeting the tumor metabolic pathway is rationally probable but practically challenging. Yet recent studies on metabolism demonstrate that tumors and T cells compete for glucose and methionine and that this competition can affect the functions of tumor-infiltrating lymphocytes (TILs), raising the notion that metabolic biomarkers may be crucial factors in antitumor immune responsiveness.[30] 1C pathways are upregulated in multiple tumor types, with several key enzymes such as PHGDH, SHMT2, methylenetetrahydrofolate dehydrogenase 2 (MTHFD2), thymidylate synthase (TYMS), and dihydrofolate reductase (DHFR) implicated in regulating cancer cell proliferation and being possible drug targets.[31–34] However, the role of only a limited number of 1C pathway members in tumor, especially human HCC, has been explored and the possible role of cancer cell 1C metabolism in modulating local immune environments has rarely been documented. Our current study uncovered a novel role of PSPH from 1C metabolism in facilitating HCC progression through engendering a myeloid-cell-high, effector-T cell-low tumor microenvironment. Notably, this enzyme exerted different effects on the expression of CCL2 and CXCL10 by cancer cells. The downregulation of CXCL10 was mediated by SAM, downstream of the 1C pathway, presumably through H3K27me3-related regulation of gene expression, while the upregulation of CCL2 was mediated by GSH, which neutralized ROS and thus released the activation of the STAT3 signaling pathway. Importantly, downregulation of PSPH significantly enhanced the antitumor efficacy of anti-PD-1 therapy in mice in vivo, suggesting it is a biomarker as well as a promising drug target for the future design of combination therapies.

Our results showed that sh*PSPH* did not impact hepatoma cell growth per se, which were different from some previous reports showing that PSPH could directly regulate HCC cancer cell behaviors.[35 36] The specific cell lines or nutrient-deprived conditions employed by those studies might partially explain the different results. It is worth noting that our in vitro experiments used the complete medium instead of the serine low or free medium, although limited serine supplement might presumably bear more resemblance to the in vivo nutrient-stressed tumor microenvironment, and serine incomplete medium might compensate for the downregulation of PSPH with regards to its downstream effects.[37] While the in vivo tumor microenvironments of HCC might exhibit serine stress to some extent due to demands from DNA synthesis, the highly heterogeneous tumor spatio-environments are hard to simulate, and

given the anticipated antiproliferation effects of disruption of 1C metabolism on cancer cells under serine-depleted conditions, a complete medium might be more suitable in terms of dissecting the effects of 1C pathway on cancer cell proliferation from its possible direct role in regulating chemokine expression by these cells. As to why didn't the serine in the complete medium compensate for the sh*PSPH*-induced loss of de novo synthesized serine while observing the downstream functions of PSPH, we hypothesized that while sh*PSPH* did regulate CXCL10 and CCL2 through its downstream SAM and GSH, respectively, under stress due to the loss of de novo synthesis of serine, the external serine from the medium might preferentially fuel the supply for DNA synthesis, so the cancer cells can keep their growth as observed, which means that downstream pathways other than DNA synthesis might not be sufficiently compensated by serine from the complete medium.[38] But such a hypothesis surely requires further exploration and validation.

The current study provided evidence that on cytokine stimulation, PSPH in cancer cells could increase CCL2 expression while inhibiting their production of CXCL10, thus presumably tilting the balance of immune composition towards a myeloid-biased direction in HCC tumor microenvironments, leading to disease progression or ICB resistance.[23 39] Such finding was consistent with recent reports that a myeloid-biased immune signature was associated with a shift in the myeloid response balance from antitumor to pro-tumor activities, accompanied by enhanced $CD8^+$ T cell exhaustion patterns, and effectively predicted recurrence and survival of patients with HCC.[40] We hypothesize that levels of PSPH expression might therefore serve as a novel biomarker for stratifying patients with HCC for ICB therapy, although the cut-off might need to be adjusted according to different patient cohorts. About 80% of the patients enrolled in the current study exhibited a relative increase of PSPH expression in tumor than in respective non-tumor liver tissue, which might partially explain, if the hypothesis holds true by and large, the relatively low responsiveness to ICB therapy of patients with HCC. Moreover, levels of PSPH not only correlated with those of chemokines expression and myeloid/effector T cells infiltration in HCC tumor tissue, but also associated with AST/ALT, P^+, and LDH in peripheral blood of the same patients, indicating that, if a correlation model could be further established, levels of PSPH expression in tumor tissue might be able to be translated into/predicted by a combination of peripheral signatures of patients with HCC, which might be of more practical value in terms of clinical usage.

In addition to biomarker, PSPH could also serve as a direct target for immunotherapy in combination with ICB agents. sh*PSPH* could lower levels of CCL2 expression and macrophages infiltration while increasing levels of CXCL10 expression and $CD8^+$ T cells infiltration. Such shift from myeloid-biased to effector T cell-rich composition in tumor microenvironments might prime the tumor for a better response to immune therapy, and accordingly, sh*PSPH* did sensitize hepatoma to the treatment of anti-PD-1 antibodies in mice in vivo. Notably, no commercial inhibitor selectively targeting PSPH is available currently, so we went a step further to try to figure out whether some currently approved drugs with broad targets might potentially affect the expression of PSPH in cancer cells, and thus represent alternatives to PSPH inhibitors. Interestingly, our results showed that metformin, an antidiabetes and antiaging drug without direct effect on hepatoma cells, could mimic the effects of sh*PSPH* by inhibiting PSPH expression in cancer cells, downregulating CCL2 levels and macrophages infiltration, upregulating CXCL10 levels and $CD8^+$ T cells infiltration in tumor tissues, and subsequently inhibiting tumor growth in mice in vivo. Importantly, a combination of metformin and anti-PD-1 antibodies exhibited better antitumor effects compared with either treatment alone, representing another similarity between the effects of metformin and sh*PSPH*. Of course, ultimately, metformin might or might not act through PSPH to inhibit tumor growth, and the several effects of metformin observed might just be correlations instead of cause-effect relationships. However, for metformin, our current study provided a piece of evidence for its potential repurposed use in the treatment of human HCC, and for PSPH, the effects of metformin arguably provided another layer of evidence for its role in modulating HCC tumor immune environments. Of note, different from a previous study finding that metformin had effects on both energy intake and energy expenditure that were dependent on growth differentiation factor 15 (GDF15),[41] no significant difference between the sh*PLKO*-Hepa1-6 and sh*PSPH*-Hepa1-6 tumors in terms of their GDF15 levels were found in the current study (data not shown), indicating that metformin might function via distinct mechanisms in different experimental/clinical models.

There are several unsolved problems in the current study. For example, it is unclear what factors might be responsible for determining levels of PSPH expression by HCC cancer cells—possible clues include the availability of extracellular serine or other nutrition-related signaling pathways shifts. As mentioned above, possible mechanisms mediating the effects of metformin on PSPH expression and tumor progression also warrant further exploration. Nevertheless, our current study unveiled a novel and interesting role of PSPH, a member of the 1C metabolism pathway, in modulating immune composition—specifically, regulating the production of CCL2 and CXCL10, and influencing the subsequent balance of myeloid and effector T cells infiltration—in HCC tumor microenvironments. PSPH thus represented a biomarker as well as a potential target for combined therapy with ICB agents in the treatment of HCC.

Acknowledgements The authors thank the Cancer Center of Sun Yat-sen University and Sun Yat-sen Memorial Hospital for their assistance in processing clinical samples. The authors specially thank Ling Yan Zhu (School of Life Sciences, Sun Yat-sen University) for helping with the flow cytometry and cell sorting procedure.

Contributors Z-PP designed the experiments, processed tissues, performed flow cytometry/real-time PCR/mouse experiments, collected data, and participated in the writing of the paper. X-CL performed immunohistochemical, immunofluorescence staining, and mouse experiments. Y-HR, DJ and A-QH performed ELISA and western blotting. W-RN and Z-ZJ helped and performed GO/GSEA analysis. LZ and YW planned and supported the project, analyzed data, and wrote the paper. YW was responsible for the overall content as the guarantor.

Funding This work was supported by project grants from the National Key R&D Program of China (2021YFC2300601), the National Natural Science Foundation of China (82071743, 32230034), Guangdong TeZhi Program (2019TQ05Y677), Fundamental Research Funds for the Central Universities (22yklj03, 22qntd2619), and Guangdong Science and Technology Department (2020B1212060031).

Competing interests None declared.

Patient consent for publication Not applicable.

Ethics approval This study involves human participants. All samples were anonymously coded in accordance with local ethical guidelines (as stipulated by the Declaration of Helsinki). The study protocol was approved by the Institutional Review Board of Sun Yat-Sen University Cancer Center (GZR2020-199). Written informed consent was obtained from each patient before taking part in the study.

Provenance and peer review Not commissioned; externally peer reviewed.

Data availability statement Data are available in a public, open access repository. All data relevant to the study are included in the article or uploaded as supplementary information. The publicly available microarray data sets analyzed in this study from The Cancer Genome Atlas (TCGA) were downloaded from the data portal of Genomic Data Commons (GDC, https://portal.gdc.cancer.gov/). The sequencing data have been deposited at the Gene Expression Omnibus with access number GSE193329. The other data generated in this study are included in the article or uploaded as supplementary materials.

ORCID iDs
Limin Zheng http://orcid.org/0000-0002-8281-1450
Yan Wu http://orcid.org/0000-0002-9022-9794

REFERENCES

1 Ducker GS, Rabinowitz JD. One-carbon metabolism in health and disease. *Cell Metab* 2017;25:27–42.
2 Newman AC, Maddocks ODK. Serine and functional metabolites in cancer. *Trends Cell Biol* 2017;27:645–57.
3 Yang M, Vousden KH. Serine and one-carbon metabolism in cancer. *Nat Rev Cancer* 2016;16:650–62.
4 Lan X, Field MS, Stover PJ. Cell cycle regulation of folate-mediated one-carbon metabolism. *Wiley Interdiscip Rev Syst Biol Med* 2018;10:e1426.
5 Reina-Campos M, Linares JF, Duran A, *et al*. Increased serine and one-carbon pathway metabolism by PKCλ/ι deficiency promotes neuroendocrine prostate cancer. *Cancer Cell* 2019;35:385–400.
6 Ju H-Q, Lu Y-X, Chen D-L, *et al*. Modulation of redox homeostasis by inhibition of MTHFD2 in colorectal cancer: mechanisms and therapeutic implications. *J Natl Cancer Inst* 2019;111:584–96.
7 Mentch SJ, Locasale JW. One-Carbon metabolism and epigenetics: understanding the specificity. *Ann N Y Acad Sci* 2016;1363:91–8.
8 Locasale JW. Serine, glycine and one-carbon units: cancer metabolism in full circle. *Nat Rev Cancer* 2013;13:572–83.
9 Zarou MM, Vazquez A, Vignir Helgason G. Folate metabolism: a re-emerging therapeutic target in haematological cancers. *Leukemia* 2021;35:1539–51.
10 Arlt B, Zasada C, Baum K, *et al*. Inhibiting phosphoglycerate dehydrogenase counteracts chemotherapeutic efficacy against MYCN-amplified neuroblastoma. *Int J Cancer* 2021;148:1219–32.
11 Zhang B, Zhang Y, Li R, *et al*. The efficacy and safety comparison of first-line chemotherapeutic agents (high-dose methotrexate, doxorubicin, cisplatin, and ifosfamide) for osteosarcoma: a network meta-analysis. *J Orthop Surg Res* 2020;15:51.
12 Ribas A, Wolchok JD. Cancer immunotherapy using checkpoint blockade. *Science* 2018;359:1350–5.
13 Nagarsheth N, Wicha MS, Zou W. Chemokines in the cancer microenvironment and their relevance in cancer immunotherapy. *Nat Rev Immunol* 2017;17:559–72.
14 Zhao B, Zhao H, Zhao J. Efficacy of PD-1/PD-L1 blockade monotherapy in clinical trials. *Ther Adv Med Oncol* 2020;12:1758835920937612.
15 Tang H, Wang Y, Chlewicki LK, *et al*. Facilitating T cell infiltration in tumor microenvironment overcomes resistance to PD-L1 blockade. *Cancer Cell* 2016;29:285–96.
16 Gibney GT, Weiner LM, Atkins MB. Predictive biomarkers for checkpoint inhibitor-based immunotherapy. *Lancet Oncol* 2016;17:e542–51.
17 Ma L, Wang L, Khatib SA, *et al*. Single-cell atlas of tumor cell evolution in response to therapy in hepatocellular carcinoma and intrahepatic cholangiocarcinoma. *J Hepatol* 2021;75:1397–408.
18 Peng D, Kryczek I, Nagarsheth N, *et al*. Epigenetic silencing of Th1-type chemokines shapes tumour immunity and immunotherapy. *Nature* 2015;527:249–53.
19 Kurniawan H, Franchina DG, Guerra L, *et al*. Glutathione restricts serine metabolism to preserve regulatory T cell function. *Cell Metab* 2020;31:920–36.
20 Krall AS, Mullen PJ, Surjono F, *et al*. Asparagine couples mitochondrial respiration to ATF4 activity and tumor growth. *Cell Metab* 2021;33:1013–26.
21 Corominas-Faja B, Quirantes-Piné R, Oliveras-Ferraros C, *et al*. Metabolomic fingerprint reveals that metformin impairs one-carbon metabolism in a manner similar to the antifolate class of chemotherapy drugs. *Aging (Albany NY)* 2012;4:480–98.
22 Luciano-Mateo F, Hernández-Aguilera A, Cabre N, *et al*. Nutrients in energy and one-carbon metabolism: learning from metformin users. *Nutrients* 2017;9:121.
23 Chen D-P, Ning W-R, Jiang Z-Z, *et al*. Glycolytic activation of peritumoral monocytes fosters immune privilege via the PFKFB3-PD-L1 axis in human hepatocellular carcinoma. *J Hepatol* 2019;71:333–43.
24 Tumeh PC, Harview CL, Yearley JH, *et al*. Pd-1 blockade induces responses by inhibiting adaptive immune resistance. *Nature* 2014;515:568–71.
25 Ries CH, Cannarile MA, Hoves S, *et al*. Targeting tumor-associated macrophages with anti-csf-1r antibody reveals a strategy for cancer therapy. *Cancer Cell* 2014;25:846–59.
26 Chow A, Schad S, Green MD, *et al*. Tim-4+ cavity-resident macrophages impair anti-tumor CD8+ T cell immunity. *Cancer Cell* 2021;39:973–988.
27 Lavin Y, Kobayashi S, Leader A, *et al*. Innate immune landscape in early lung adenocarcinoma by paired single-cell analyses. *Cell* 2017;169:750–65.
28 Hensley CT, Faubert B, Yuan Q, *et al*. Metabolic heterogeneity in human lung tumors. *Cell* 2016;164:681–94.
29 Thorsson V, Gibbs DL, Brown SD, *et al*. The immune landscape of cancer. *Immunity* 2018;48:S1074-7613(18)30121-3:812–830..
30 Bian Y, Li W, Kremer DM, *et al*. Cancer SLC43A2 alters T cell methionine metabolism and histone methylation. *Nature* 2020;585:277–82.
31 Wei Z, Song J, Wang G, *et al*. Deacetylation of serine hydroxymethyltransferase 2 by SIRT3 promotes colorectal carcinogenesis. *Nat Commun* 2018;9:4468.
32 Zhao M, Tan B, Dai X, *et al*. DHFR/TYMS are positive regulators of glioma cell growth and modulate chemo-sensitivity to temozolomide. *Eur J Pharmacol* 2019;863:172665.
33 Issaq SH, Mendoza A, Kidner R, *et al*. EWS-FLI1-regulated serine synthesis and exogenous serine are necessary for Ewing sarcoma cellular proliferation and tumor growth. *Mol Cancer Ther* 2020;19:1520–9.
34 Li G, Wu J, Li L, *et al*. P53 deficiency induces MTHFD2 transcription to promote cell proliferation and restrain DNA damage. *Proc Natl Acad Sci U S A* 2021;118:e2019822118.

35 Sun L, Song L, Wan Q, *et al*. CMyc-mediated activation of serine biosynthesis pathway is critical for cancer progression under nutrient deprivation conditions. *Cell Res* 2015;25:429–44.
36 Zhang J, Wang E, Zhang L, *et al*. PSPH induces cell autophagy and promotes cell proliferation and invasion in the hepatocellular carcinoma cell line Huh7 via the AMPK/mTOR/ULK1 signaling pathway. *Cell Biol Int* 2021;45:305–19.
37 Montrose DC, Saha S, Foronda M, *et al*. Exogenous and endogenous sources of serine contribute to colon cancer metabolism, growth, and resistance to 5-fluorouracil. *Cancer Res* 2021;81:2275–88.
38 Sullivan MR, Mattaini KR, Dennstedt EA, *et al*. Increased serine synthesis provides an advantage for tumors arising in tissues where serine levels are limiting. *Cell Metab* 2019;29:1410–21.
39 Ning W-R, Jiang D, Liu X-C, *et al*. Carbonic anhydrase XII mediates the survival and prometastatic functions of macrophages in human hepatocellular carcinoma. *J Clin Invest* 2022;132:e153110.
40 Wu C, Lin J, Weng Y, *et al*. Myeloid signature reveals immune contexture and predicts the prognosis of hepatocellular carcinoma. *J Clin Invest* 2020;130:4679–93.
41 Coll AP, Chen M, Taskar P, *et al*. GDF15 mediates the effects of metformin on body weight and energy balance. *Nature* 2020;578:444–8.

Supplementary Materials for

Down-regulation of Phosphoserine Phosphatase Potentiates Tumor Immune Environments to Enhance Immune Checkpoint Blockade Therapy

Zhi-Peng Peng[#], Xing-Chen Liu[#], Yong-Hao Ruan, Da Jiang, Ai-Qi Huang, Wan-Ru Ning, Ze-Zhou Jiang, Limin Zheng[*], Yan Wu[*]

[#] These authors contributed equally

*Corresponding author

Email: wuyan32@mail.sysu.edu.cn (Y.W.)

zhenglm@mail.sysu.edu.cn (L.Z.)

Supplementary materials include:

Supplementary Materials and Methods

Supplementary Figures: Fig. S1 to S12

Supplementary Tables: Table S1 to S5

Peng Z-P, *et al. J Immunother Cancer* 2023; 11:e005986. doi: 10.1136/jitc-2022-005986

Supplementary Materials and Methods

Cell lines

Hepa1-6 mouse hepatocellular carcinoma cells, PLC/PRF/5 human hepatocellular carcinoma cells, SNU449 human hepatocellular carcinoma cells, and HEK 293T cells were purchased from American Type Culture Collection (ATCC). Their identities were verified by the STR method. Hepa1-6 and HEK 293T were grown in DMEM (C11995500BT, Gibco), PLC/PRF/5 and SNU449 were grown in RPMI 1640 (C11875500BT, Gibco), with 10% fetal bovine serum (FBS, 10099-141, Gibco), 100 units/ml penicillin (AP231, GENVIEW) and 100 μg/ml streptomycin antibiotics (AS325, GENVIEW). All cell lines were regularly tested for mycoplasma contamination using the single-step polymerase chain reaction (PCR) method.

Plasmids, shRNA and lentivirus production

pLKO.1 plasmid was obtained from Addgene (10878). Lentiviral shRNAs (Supplementary Table S3) were purchased from Sangon Biotech (Shanghai, China). For lentivirus productions, the lentivirus expression vector containing the target sequence was co-transfected into HEK 293T cells with packaging plasmid psPAX2 (Addgene, 12260) and envelope plasmid pMD2.G (Addgene, 12259) by Polyethylenimine Linear (PEI, 24765, Polysciences). The lentivirus supernatant was harvested and stored in aliquots at -80°C until use. The stable PSPH knockdown cell lines were established by infecting PLC/PRF/5 and SNU449 cells with lentivirus expressing the target sequence and selected by puromycin treatment.

In vitro culture of PLC/PRF/5, SNU449 and Hepa1-6

In some experiments, PLC/PRF/5 and SNU449 were left untreated or treated with human recombinant TNF-α (5 ng/ml, 210-TA-010, R&D Systems), human recombinant IL-1β (5 ng/ml, 201-LB-005, R&D Systems), or human recombinant IFN-γ (5 ng/ml, 285-IF-100, R&D Systems) for 24 hours. In some experiments, PLC/PRF/5 and SNU449 were stimulated with human recombinant TNF-α in the presence or absence of S-(5′-Adenosyl)-L-methionine (SAM, 2 mM, A7007, Sigma-Aldrich), N-Acetyl-L-cysteine (NAC, 1mM for SNU449; 5mM for PLC/PRF/5, A7250, Sigma-Aldrich), 3-Deazaadenosine hydrochloride (3-DZA, 5 μM, HY-W013332A, MCE), AG490 (10 μM, HY-12000, MCE), or DMSO for 24 hours. In some other experiments, Hepa1-6 was treated with Metformin (60mM, HY-17471A, MCE) for 12 hours.

UHPLC-MRM-MS/MS analysis of metabolites

Fresh HCC tumor and paired non-tumor liver tissues were cut into small pieces and stored at -80°C before use. UHPLC-MRM-MS/MS was performed by Shanghai Biotree Biotech Limited Company (Shanghai, China), and the abundance of metabolites (D-3-Phosphoserine, Glycine, L-Serine, L-Methionine) was measured and compared to internal standard controls according to protocols.

Isolation of leukocytes from tissues

For isolation of tumor-infiltrating leukocytes from mouse tumors, fresh tumors were cut into small pieces and digested in RPMI 1640 medium supplemented with 0.002% DNase I (DN25, Sigma-Aldrich), 0.05% collagenase IV (C5138, Sigma-Aldrich), 50 μg/ml hyaluronidase (H1136, Sigma-Aldrich), 30 μg/ml Collagenase XI (C7657,

Sigma-Aldrich), 20% FBS, 100U/ml penicillin and 100μg/ml streptomycin at 37°C for 40 minutes. Dissociated cells were separated by Ficoll density-gradient centrifugation. Leukocytes were stained with PE/Cyanine7-conjugated anti-mouse CD11b (101216, Biolegend), BV421-conjugated anti-mouse Ly6C (128032, Biolegend), FITC-conjugated anti-mouse Gr-1 (11-5931-85, eBioscience), and PE-CF594-conjugated anti-mouse Ly6G antibodies (562700, Biolegend). $Ly6C^+$ monocytes and $F4/80^+$ macrophages were then purified using a MoFlo XDP Cell Sorter (Beckman Coulter, Brea, U.S.). The purified cells were then used for direct analysis, or in vivo cell transfusion experiments.

The Cancer Genome Atlas (TCGA) data analysis

The TCGA clinical data were downloaded from the data portal of Genomic Data Commons. Gene expression profiles of 50 patients with paired tumor and non-tumor data were enrolled for analysis.

Quantitative real-time PCR (Q-PCR)

Total RNA was extracted using TRIzol reagent (AM9738, Life Technologies) and then used to synthesize cDNA with 5X All-In-One RT MasterMix (G486, Abm). Sequences of the primers used for PCR analysis were listed in Supplementary Table S3. Quantitative PCR was performed according to a standard protocol using the SYBR Green Real-Time PCR Mix (QPS-201, TOYOBO) in LightCycler 480 System (Roche, Basel, Switzerland). To determine the relative fold change of different genes, their levels of expression were normalized to those of β-actin.

Western blotting (WB)

Primary antibodies used included: PSPH Rabbit Polyclonal antibody (14513-1-AP, Proteintech), MTHFD1L Rabbit Polyclonal antibody (16113-1-AP, Proteintech), ALDH1L2 Rabbit Polyclonal antibody (21391-1-AP, Proteintech), MAT2A Rabbit Polyclonal antibody (55309-1-AP, Proteintech), ALDH1L1 Rabbit Polyclonal antibody (17390-1-AP, Proteintech), MAT1A Rabbit Polyclonal antibody (12395-1-AP, Proteintech), H3K27me3 Rabbit Monoclonal antibody (9733, Cell Signaling Technology), Histone H3 Rabbit Monoclonal antibody (4499, Cell Signaling Technology), phospho-STAT3^{Tyr705} Rabbit Monoclonal antibody (9145, Cell Signaling Technology, Danvers, U.S.), STAT3 Mouse Monoclonal Antibody (9139, Cell Signaling Technology), β-actin Mouse Monoclonal Antibody (ab8226, Abcam). HRP-linked goat anti-rabbit/mouse IgG antibodies were purchased from Cell Signaling Technology.

Immunohistochemistry (IHC) staining

Paraffin-embedded and formalin-fixed samples were cut into 4 μm sections. After incubation with primary antibodies against PSPH (14513-1-AP, Proteintech), sections were stained with corresponding secondary antibodies and visualized with diaminobenzidine and 3-amino-9-ethylcarbazole in an Envision System. The intensity of protein expression was quantified using ImagePro Plus software (Media Cybernetics, Maryland, U.S.).

Multiplex immunofluorescence (IF) staining

For multiplex immunofluorescence analysis of patient samples, Paraffin-embedded and formalin-fixed samples were cut into 4 μm sections. The sections were incubated

with primary antibodies against PSPH (14513-1-AP, Proteintech), F4/80 (70076, Cell Signaling Technology), CD8a (98941, Cell Signaling Technology), Ly6C (ab15627, Abcam), or PSPH (14513-1-AP, Proteintech), CD68 (M087629, Dako), CD8a (85336, Cell Signaling Technology), H3K27me3 (9733, Cell Signaling Technology), phospho-STAT3^{Tyr705} (9145, Cell Signaling Technology). Immunofluorescence signals were amplificated by a tyramide signal amplification kit (PPK007100100, Panovue) for visualization. Nuclei were counterstained with DAPI (10236276001, Roche).

Immunofluorescence staining images were visualized by the ZEISS microscope (LSM780, Germany). The intensity of protein expression was evaluated using Zeiss ZEN software (LSM780, Germany), and positive cells were quantified using ImagePro Plus software (Media Cybernetics, Maryland, U.S.). Results were expressed as mean ± SEM in high-powered fields.

Flow cytometry

Cell surface markers were determined by direct staining with anti-mouse CD45-BV570 (103135, Biolegend), anti-mouse Ly-6G-PE-cf594 (562700, BD Biosciences), anti-mouse Ly-6C-BV421 (128032, Biolegend), anti-mouse CD11b-AF700 (101222, Biolegend), anti-mouse F4/80-APC (123116, Biolegend), anti-mouse CD3-FITC (100203, Biolegend), anti-mouse CD8a-PE (100708, Biolegend). In some experiments, to measure intracellular perforin or granzyme B production, lymphocytes were cultured at 37°C for 12 hours, stained with surface markers, fixed, permeabilized with IntraPre Reagent (A07803, Beckman), and further stained with anti-mouse Perforin-APC (154404, Biolegend) and anti-mouse

Granzyme B-PC7 (372214, Biolegend). Hepa1-6 apoptosis was quantified using an annexin V apoptosis detection kit (K201, Biovision) following the manufacturer's instructions. Data were acquired with CytoFLEXS flow cytometer (Beckman Coulter, Brea, U.S.) and evaluated with FlowJo software version V10 (Tree Star, Ashland, U.S.) (Supplementary Fig. S12).

Intracellular ROS detection

PLC/PRF/5 and SNU449 cells were stimulated with human recombinant TNF-α for 24 hours, and then incubated with dichlorofluorescein diacetate (5μM, 2044-85-1, Sigma-Aldrich) for 30 minutes at 37°C. Cells were analyzed by CytoFLEXS flow cytometer (Beckman Coulter, Brea, U.S.).

Cell viability assay

sh*PLKO*-Hepa1-6 and sh*PSPH*-Hepa1-6 cells were seeded into 96-well plates (3000 cells per well) for 24 hours. In some experiments, Hepa1-6 was seeded into 96-well plates and treated with Metformin for 12 hours. 10μl CCK-8 (ab228554, Abcam) was added into 190μl medium to each well for incubation at 37°C for 2 hours, then the optical density (OD) was measured by varioskan lux (Thermo Scientific, Waltham, U.S.) at 450 nm.

Enzyme-linked immunosorbent assay (ELISA)

Concentrations of CCL2, CXCL10 (88-7399-88 / CHC2363, Invitrogen), SAM, SAH (SAM, MM-13267H1, MEIMIAN; SAH, MM-13268H1, MEIMIAN), GSH, and GSSG (GSH/GSSG, S0053, Beyotime) were determined by ELISA kits according to the manufacturer's instructions.

RNAseq and enrichment analysis

PLC/PRF/5 and SNU449 were stimulated with human recombinant TNF-α for 24 hours. RNA of the cells was extracted by TRIzol method, and RNA-sequencing was processed on an Illumina HiSeq 2500 platform (Illumina, San Diego, U.S.). The gene matrix files were generated with RNA express app (Illumina) and analyzed using T-test comparison and log2 ratio of classes. GO term Enrichment was performed using DAVID (david.ncifcrf.gov) and Gene Set Enrichment Analysis (GSEA) was performed using the GSEA v3.0 software (http://www.broadinstitute.org/gsea/index.jsp) with 1000 gene-set permutations, using the gene-ranking metric T-test with the signatures (WP_JAK_STAT_SIGNALING_PATHWAY; WP_MAPK_SIGNALING_PATHWAY; WP_PI3KAKT_SIGNALING_PATHWAY; WP_TNF_ALPHA_SIGNALING_PATHWAY).

For further details regarding the antibodies and reagents used in this study, please refer to Supplementary Table S4 and Supplementary Table S5.

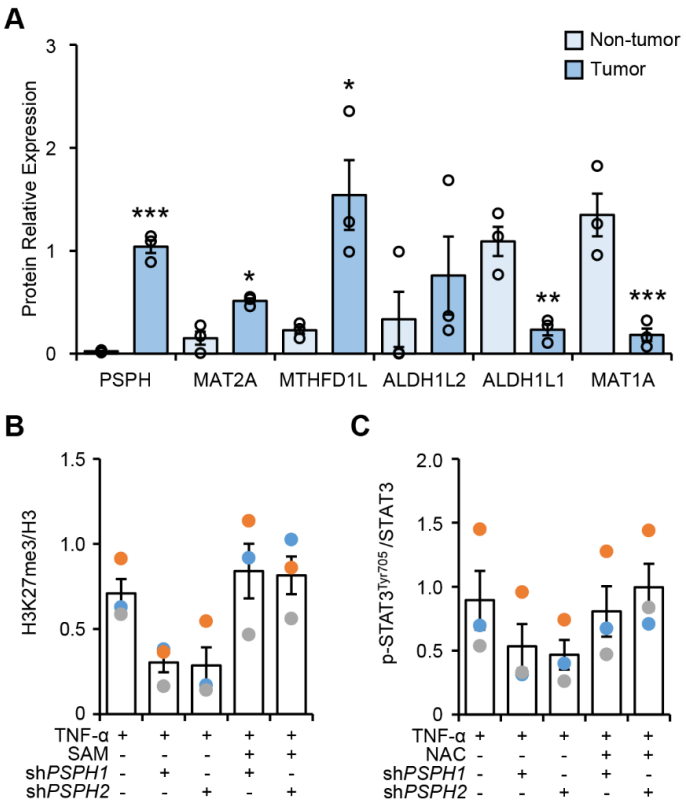

Supplementary Fig. S1 The densitometry data for Fig. 1D, 3C, and 3H.

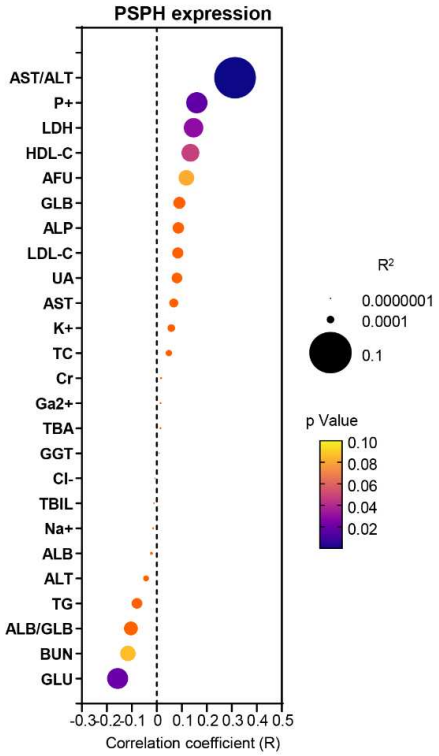

Supplementary Fig. S2 Correlation between tumor PSPH levels and peripheral markers in patients with HCC. Correlation between the levels of PSPH in tumor tissues and indicated markers in peripheral blood were monitored. n = 221. Statistical methods: Pearson correlation and linear regression analysis. AST: aspartate aminotransferase; ALT: alanine aminotransferase; LDH: lactate dehydrogenase; HDL-C: high-density lipoprotein cholesterol; AFU: alpha-L-fucosidase; GLB: globulin; ALP: a lkaline phosphatase; LHL-C: low-density lipoprotein cholesterol; UA: uric acid; TC: total cholesterol; Cr: creatinine; TBA: total bile acid; GGT: gamma-glutamyl transpeptidase; TBIL: total bilirubin; ALB: albumin; TG: triglyceride; BUN: blood urea nitrogen; GLU: glucose.

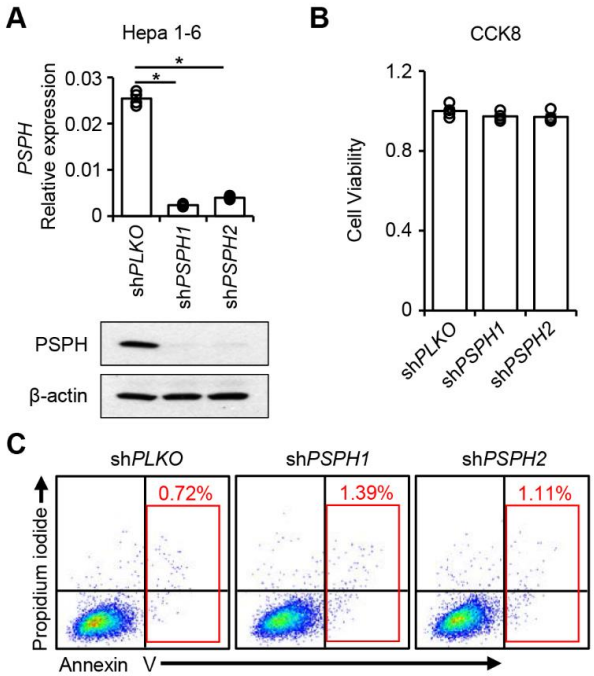

Supplementary Fig. S3 sh*PSPH* transfection does not affect tumor cell viability and apoptosis *in vitro*. A-C, Hepa1-6 cells were transfected with sh*PSPH1*, sh*PSPH2*, or sh*PLKO* control. **A,** Efficiency of sh*PSPH1* and sh*PSPH2* transfection was determined by Q-PCR and western blotting. **B,** Cell viability was measured by the CCK8 analyzing kit. **C,** Cell apoptosis was analyzed by flow cytometry. n = 4. Data are mean ± SEM. Statistical methods: Welch's t-test (**A**), Student's t test (**B**). *p < 0.05.

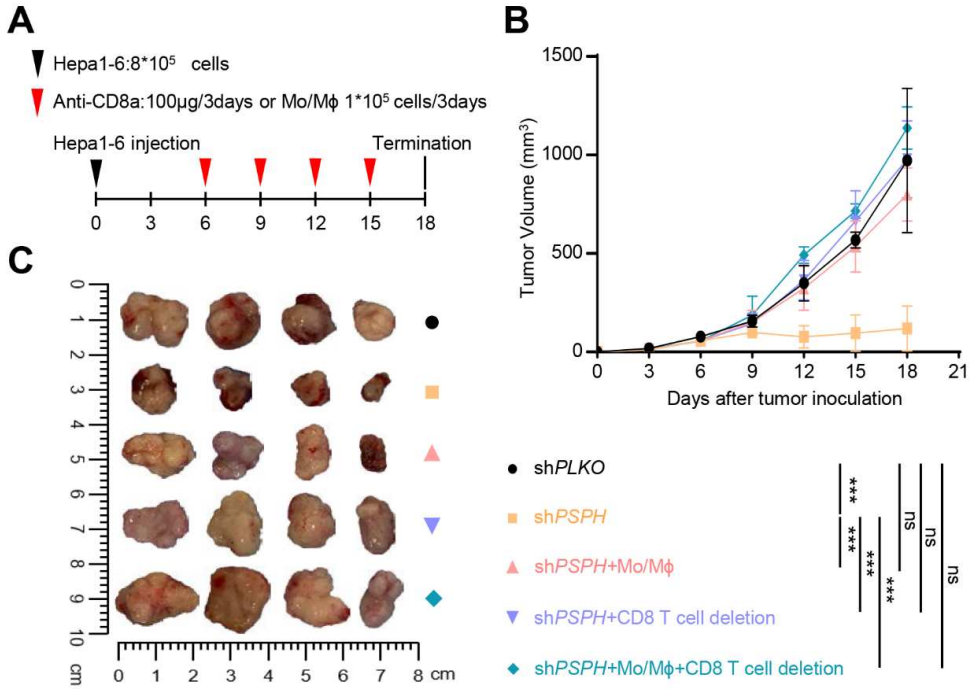

Supplementary Fig. S4 The in vivo anti-tumor effects of sh*PSPH* depended on the reduced macrophages and increased CD8$^+$ T cells infiltration. A-C, C57BL/6 Mice bearing Hepa1-6 tumors were intraperitoneally injected with anti-mouse CD8a antibodies or intratumorally injected with mice Ly6C$^+$ monocytes and F4/80$^+$ macrophages at indicated times (**A**). Tumor growth (**B, C** (day 18)) was monitored. n = 4. Statistical methods: Two-way ANOVA with Bonferroni's multiple comparisons test (**B**). ***p < 0.001; ns, no significance.

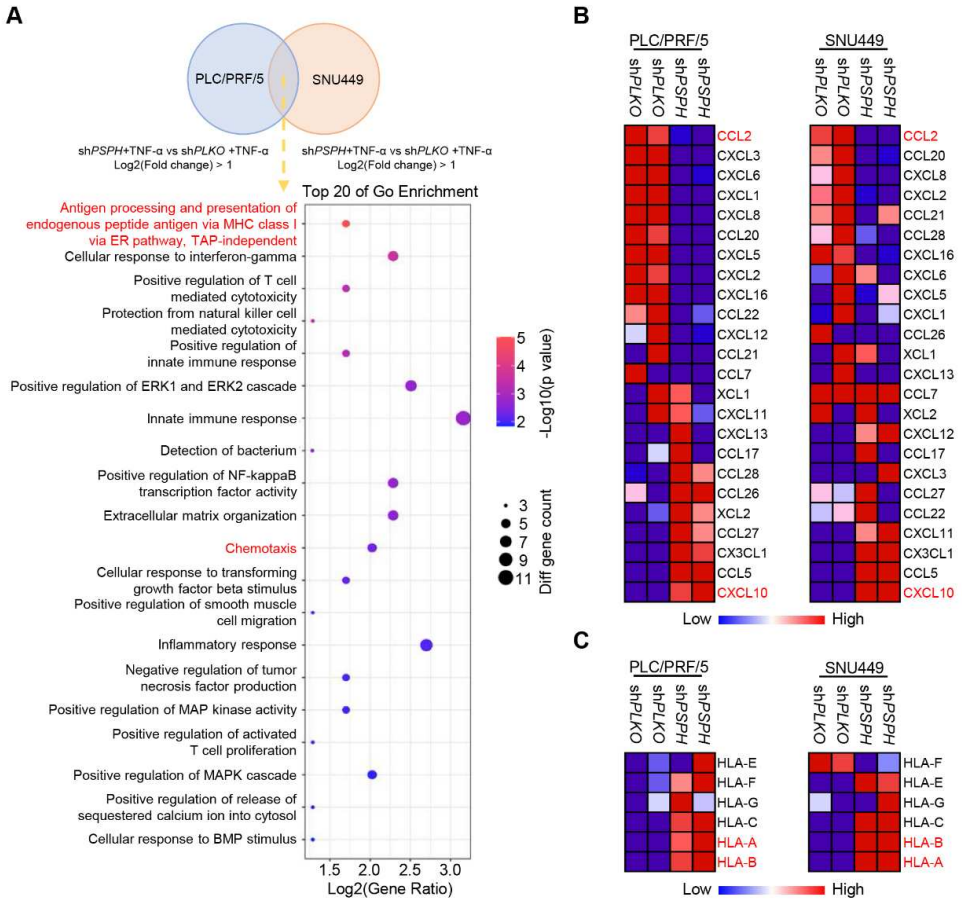

Supplementary Fig. S5 Genes differentially expressed by sh*PSPH*- and sh*PLKO*-transfected hepatoma cells. A-C, RNA-sequencing was performed to identify differentially expressed genes between the sh*PSPH* and sh*PLKO* transfected hepatoma cells (PLC/PRF/5 or SNU449 cells). The overlap genes between PLC/PRF/5 and SNU449 were subjected to the GO term enrichment analysis. n = 2 (**A**). Differentially expressed chemokines and MHC molecules were analyzed (**B-C**).

Supplementary Fig. S6

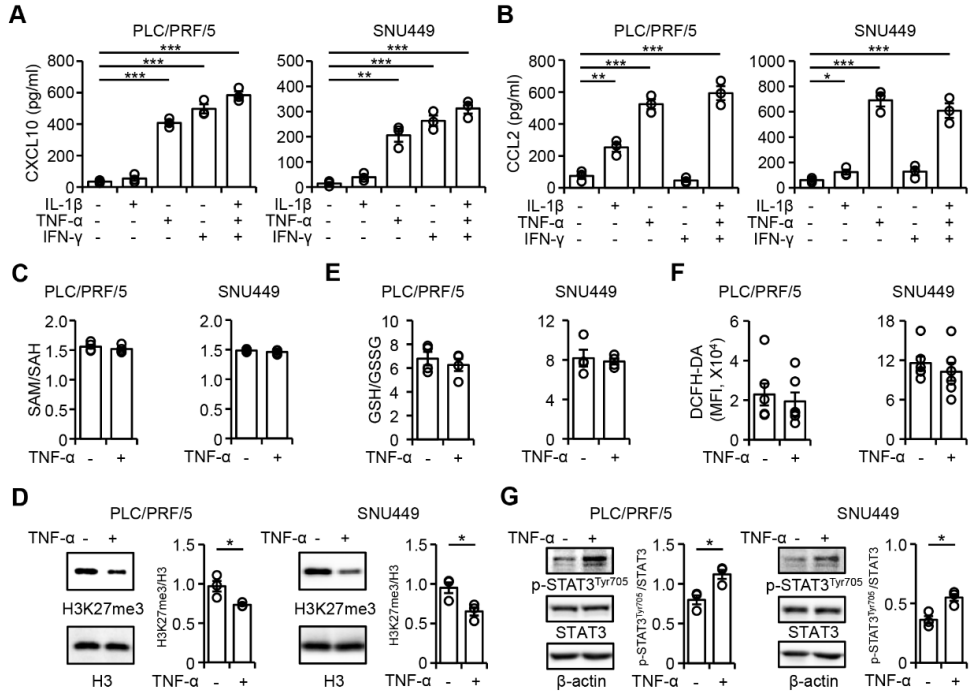

Supplementary Fig. S6 Effects of cytokines on CCL2, CXCL10, SAM/SAH, H3K27me3, GSH/GSSG, ROS, and p-STAT3^{Tyr705} expression by hepatoma cells *in vitro*. **A-B,** PLC/PRF/5 and SNU449 cells were treated with the indicated combination of cytokines. Their production of CXCL10 (**A**) and CCL2 (**B**) were measured through ELISA. n = 3. **C-G,** PLC/PRF/5 and SNU449 cells were treated with TNF-α. Levels of SAM/SAH (**C**), H3K27me3 (**D**), GSH/GSSG (**E**), ROS (**F**), and p-STAT3^{Tyr705} (**G**) in these cells were analyzed through ELISA, Western blotting, or Flow cytometry. (**C, E,** n = 4, **D, G,** n = 3, **F,** n = 6). Data are mean ± SEM. Statistical methods: Student's t test. *p < 0.05, **p < 0.01, ***p < 0.001.

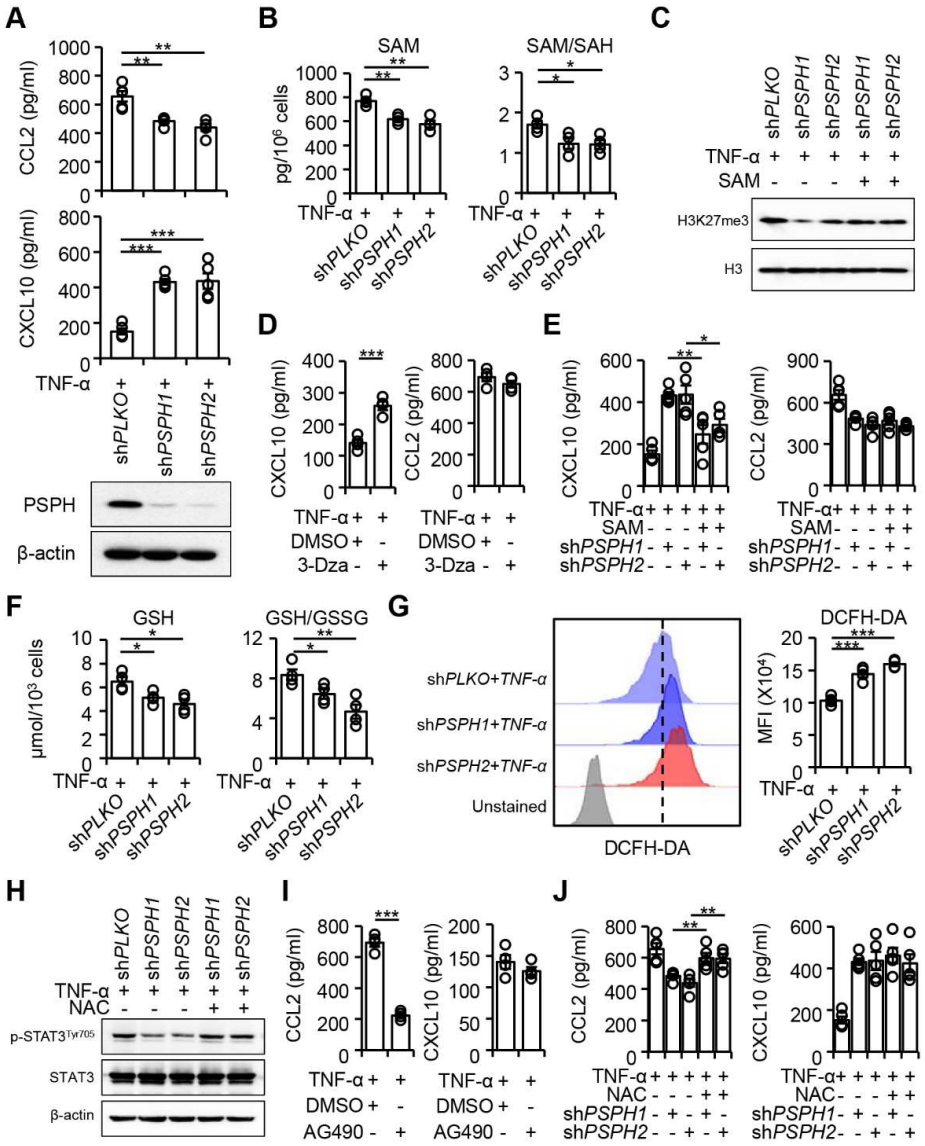

Supplementary Fig. S7 PSPH regulates tumor release of CXCL10 and CCL2 through the SAM and GSH pathways respectively. SNU449 cells were left untreated or transfected with sh*PLKO* or sh*PSPH*, and treated with TNF-α. **A,** Western blotting showed PSPH, and ELISA showed CCL2, CXCL10 levels in sh*PLKO* or sh*PSPH* tumor cells (n = 5). **B,** SAM and SAM/SAH were measured in sh*PLKO* or sh*PSPH* tumor cells (n = 4). **C,** Western blotting showed H3K27me3 in

sh*PLKO* or sh*PSPH* tumor cells, in the presence or absence of supplemented SAM (n = 3). **D-E,** ELISA showed CCL2 and CXCL10 levels in 3-Dza -treated or -untreated tumor cells (n=4, **D**), or in sh*PLKO* or sh*PSPH* transfected tumor cells, in the presence or absence of supplemented SAM (n=5, **E**). **F,** GSH and GSH/GSSG were measured in sh*PLKO* or sh*PSPH* tumor cells (n = 4). **G,** Flow cytometry analysis showed ROS levels in sh*PLKO* or sh*PSPH* tumor cells (n = 4). **H,** Western blotting showed STAT3, p-STAT3 ^{Tyr705} in sh*PLKO* or sh*PSPH* tumor cells, in the presence or absence of supplemented NAC (n = 3). **I-J,** ELISA showed CCL2 and CXCL10 levels in AG490 -treated or -untreated tumor cells (n = 4, **I**), or in sh*PLKO* or sh*PSPH* transfected tumor cells, in the presence or absence of supplemented NAC (n = 5, **J**). Data are mean ± SEM. Statistical methods: Student's t test (**A, B, D, E, F, G, I, J**). *p < 0.05, **p < 0.01, ***p < 0.001.

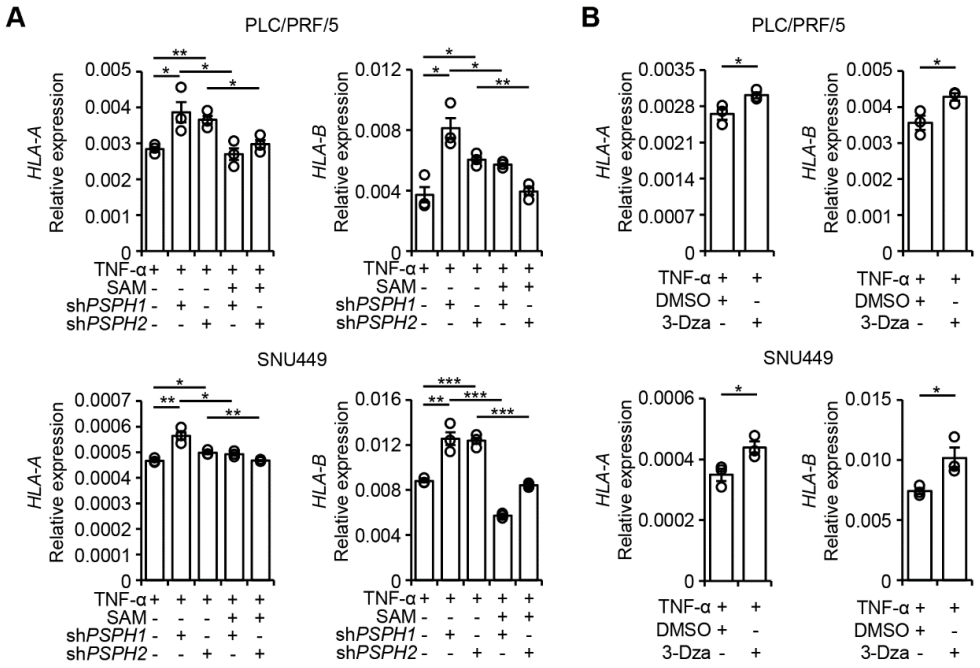

Supplementary Fig. S8 PSPH regulates tumor expression of *HLA-A* and *HLA-B* through the SAM pathway. A-B, Q-PCR analysis showed the levels of *HLA-A* and *HLA-B* expression on TNF-α-treated PLC/PRF/5 or SNU449 cells, which were transfected with sh*PLKO* or sh*PSPH*, in the presence or absence of supplemented SAM (**A**), or on TNF-α-treated PLC/PRF/5 or SNU449 cells, in the presence of DMSO or 3-Dza (**B**). n = 3. Data are mean ± SEM. Statistical methods: Student's t test (**A, B**). *P < 0.05, **P < 0.01, ***P < 0.001.

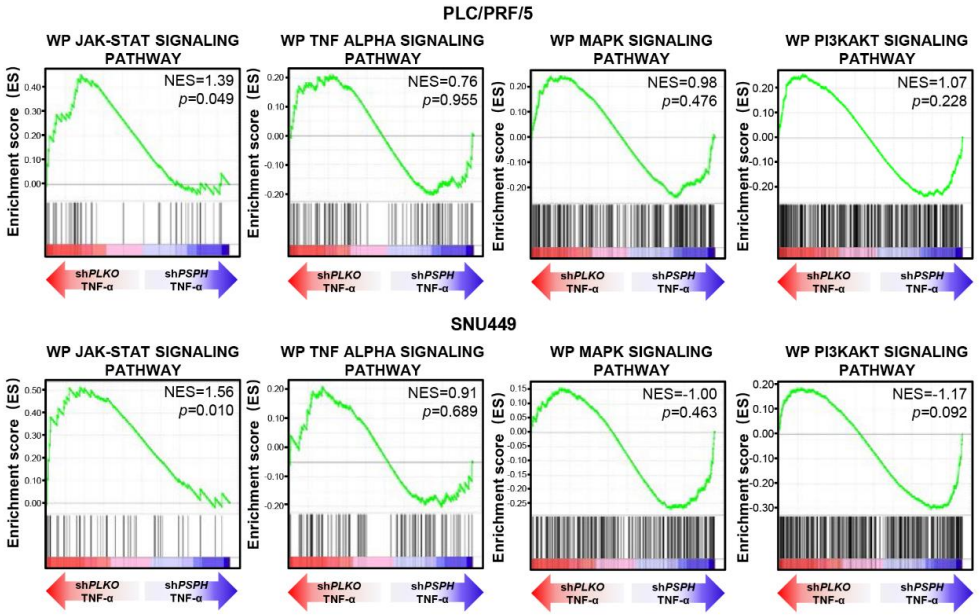

Supplementary Fig. S9 Enrichment of different signaling pathways in sh*PSPH*- vs sh*PLKO*- transfected hepatoma cells. GSEA analysis showed the enrichment of indicated signaling pathways in sh*PSPH*- vs sh*PLKO* transfected PLC/PRF/5 or SNU449 cells. n = 2.

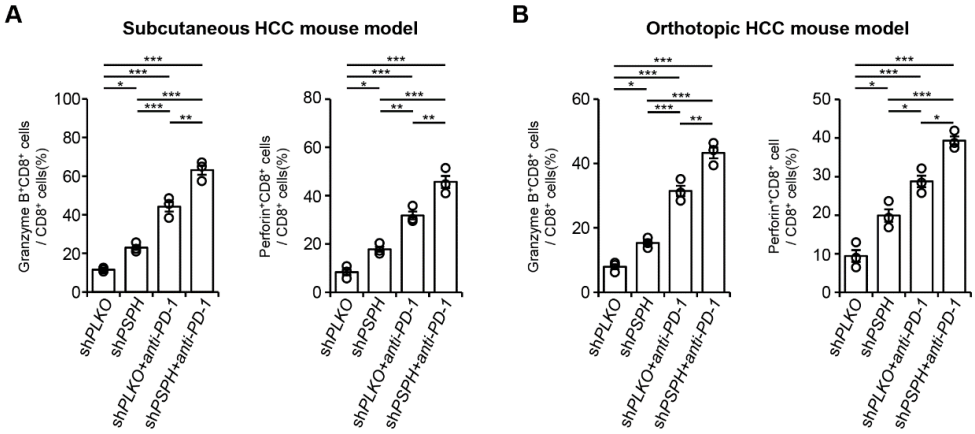

Supplementary Fig. S10 $CD8^+$ T cell activities are enhanced in sh*PSPH*-transfected Hepa1-6 tumors *in vivo*. C57BL/6 mice with established sh*PLKO* or sh*PSPH* -transfected Hepa1-6 tumors (subcutaneous (**A**) or orthotopic (**B**)) were intraperitoneally injected with or without anti-PD-1 antibodies. Flow cytometry showed the expression of Granzyme B and perforin in tumor-infiltrating $CD8^+$ T cells on Day 21. n = 3. Data are mean ± SEM. Statistical methods: Student's t test (**A, B**). *p < 0.05, **p < 0.01, ***p < 0.001; ns, no significance.

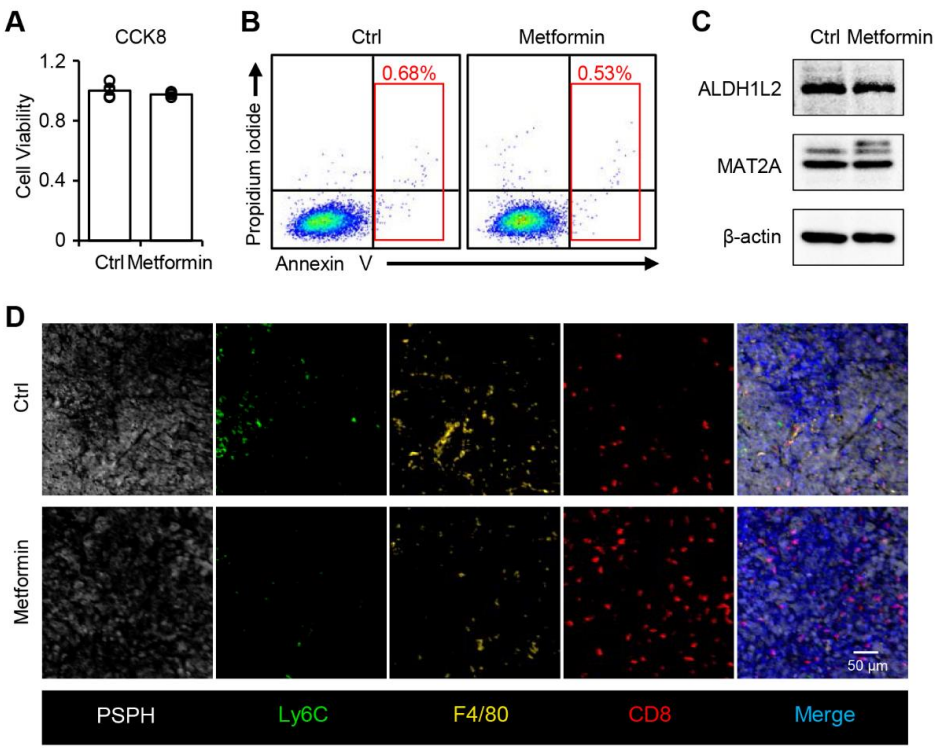

Supplementary Fig. S11 Metformin mimics the effects of sh*PSPH* in regulating tumor immune compositions. A-B, Hepa1-6 cells were treated with or without metformin for 12 hours. **A,** Cell viability was measured by CCK8 analyzing kit. **B,** Cell apoptosis was analyzed by flow cytometry. n = 4. **C,** Effects of Metformin on ALDH1L2 and MAT2A expression were determined by western blotting. n = 4. **D,** Effects of Metformin on the expression of PSPH, and the infiltrations of $Ly6C^+$ monocytes, $F4/80^+$ macrophages, and $CD8^+$ T cells in Hepa1-6 tumors in C57BL/6 mice were determined by immunofluorescent analysis. n = 3. Data are mean ± SEM. Statistical methods: Student's t test (**A**).

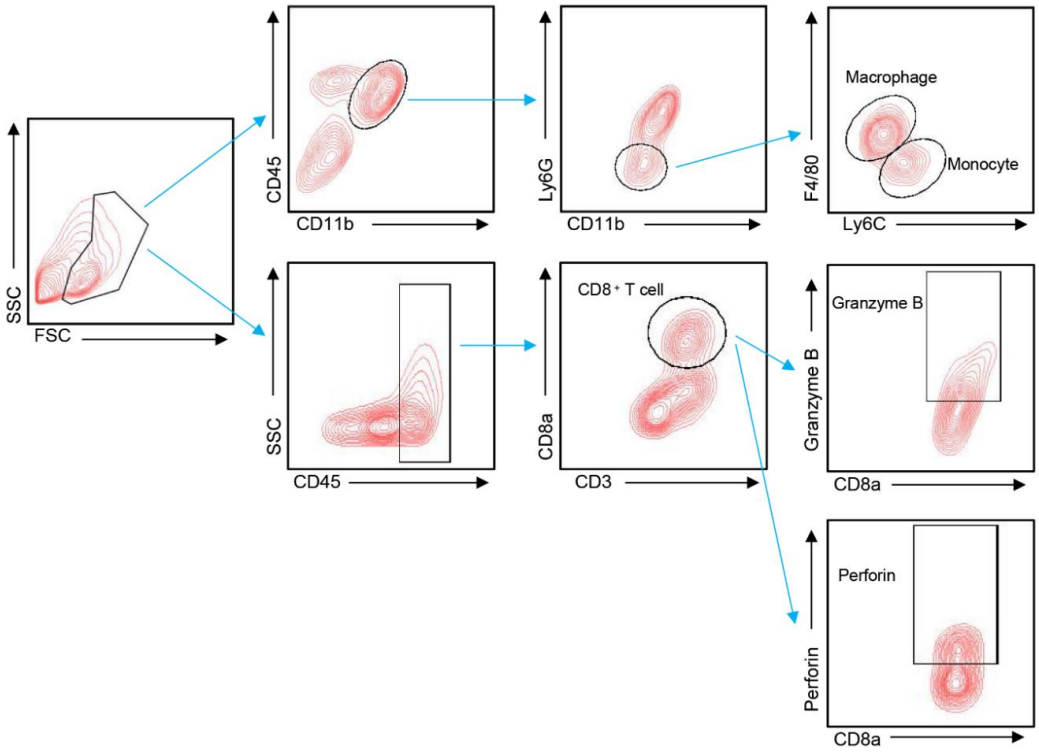

Supplementary Fig. S12 Flow cytometry gating strategy. For all the flow cytometry data in the figures, we selected CD45-BV570/CD11b-AF700/F4/80-APC triple-positive cells as macrophages and CD45-BV570/CD11b-AF700/Ly6C-BV421 triple-positive cells as monocytes. We selected CD45-BV570/CD3-FITC/CD8a-PE triple-positive cells as $CD8^+$ T cells, which were subjected to GranzymeB-PC7 and Perforin-APC analysis.

Supplementary Table S1. Clinical characteristics of HCC patients

Patients characteristics	Cohort 1	Cohort 2
No. of patients	321	30
Age, years (median, range)	49.8, 13-78	49.2, 29-69
Gender (male/female)	286/35	26/4
HBsAg (negative/positive)	32/289	5/25
ALT, U/L (median, range)	49.0, 9-713	87.0, 13-458
AFP, ng/mL (≤25/>25)	121/200	5/25
Tumor size, cm (≤5/>5)	153/168	11/19
Tumor multiplicity (solitary/multiple)	239/82	22/8
TNM stage (I/II+III)	212/109	10/20
Tumor differentiation (I+II/III+IV)	193/128	16/14
Cirrhosis (absent/present)	114/207	13/17
Fibrous capsule (absent/present)	226/95	17/13
Intrahepatic metastasis (no/yes)	205/116	20/10
Vascular invasion (absent/present)	250/71	14/16

Abbreviations: HBsAg, hepatitis B surface antigen; ALT, alanine aminotransferase; AFP, α-fetoprotein; TNM, tumor-node-metastasis.

Note: Samples from patients in Cohort 1 were used in Fig. 1J, Fig. S1, Table 1; Samples from patients in Cohort 2 were used in Fig. 1B-I, Fig. 4.

Supplementary Table S2. Univariate and multivariate analysis of factors associated with overall survival of patients with HCC.

Clinical variables	OS						
	Univariate				Multivariate		
				p value	HR	95% CI	p value
Age, years	>50	vs.	≤50	0.595			
Gender	female	vs.	male	0.314			
HBsAg	positive	vs.	negative	0.735			
ALT, U/L	>40	vs.	≤40	0.163			
AFP, ng/ml	>25	vs.	≤25	**0.014**	1.217	0.815-1.817	0.338
Tumor size, cm	>5	vs.	≤5	**<0.001**	1.454	0.985-2.145	0.060
Tumor multiplicity	multiple	vs.	solitary	**<0.001**	0.642	0.389-1.059	0.083
TNM stage	II+III	vs.	I	**<0.001**	2.872	1.720-4.794	**<0.001**
Tumor differentiation	III+IV	vs.	I+II	0.077			
Cirrhosis	present	vs.	absent	0.370			
Fibrous capsule	present	vs.	absent	0.796			
Intrahepatic metastasis	yes	vs.	no	**0.009**	1.212	0.859-1.708	0.273
Vascular invasion	yes	vs.	no	**<0.001**	1.834	1.238-2.719	**0.003**
PSPH expression	high	vs.	low	**0.001**	1.475	1.045-2.082	**0.027**

HBsAg, hepatitis B surface antigen; ALT, alanine aminotransferase; AFP, a-fetoprotein; TNM, tumor-node-metastasis; PSPH, Phosphoserine Phosphatase; HCC, hepatocellular carcinoma.

Cumulative survival time was estimated by Kaplan-Meier method, and the log-rank test was applied to compare the groups. Cox proportional hazards regression model was used to conduct a multivariate analysis of survival. p values in bold denote statistical significance.

Supplementary Table S3. Sequences for RT-PCR and shRNAs

Primers for RT-PCR

Genes		Sequences
Human *PHGDH*	Forward	GGAGGAGGAGGAGGAGATGA
	Reverse	GGCCGCTGTGAGTAGAAGTA
Human *PSAT1*	Forward	GGGAATTGCTAGCTGTTCCAG
	Reverse	TCAGCACACCTTCCTGCTTT
Human *PSPH*	Forward	ATCTCCTGACCTTGTGATCCG
	Reverse	GCTGCCGAATCCGTATTTCTAA
Human *SHMT2*	Forward	GAGCAGAGGTGGTGGATGAA
	Reverse	ATGTAGCCGTGGGTGAGATG
Human *MTHFD2*	Forward	TGGCTGCGACTTCTCTAATGT
	Reverse	CACTTCCTGCTTGATCTGCTG
Human *MTHFD1L*	Forward	CAACATCAAGTGCCGAGCTT
	Reverse	AAGAGGAACACCAGCCGTTA
Human *ALDH1L2*	Forward	TAACACATACAACAAGACAGAT
	Reverse	ATATTCATTTAGAGCTTCCTCA
Human *MTHFD1*	Forward	CCTGGCTCTCACCACTTCTC
	Reverse	ATCCTGCTTCCGTCACTACAA
Human *ALDH1L1*	Forward	GCCTGGCTTCTGGTGTCTTC
	Reverse	GCCACGTCGGTCTTGTTGTA
Human *SHMT1*	Forward	CCCGAAACCTGGAATATG
	Reverse	ATGGCAGTGTTCAAATGG
Human *MTHFR*	Forward	CTACCTCACCTGCCAGTATCTT
	Reverse	AAGCCACCACCAAACCAAAC
Human *MAT1A*	Forward	CGTGAGTGGAGAAGTGTGAGA
	Reverse	CCGATGTGCTTGATGGTGTC
Human *MAT2A*	Forward	ACAATCTACCACCTACAGCC
	Reverse	CCAACGAGCAGCATAAGC
Human *CCL2*	Forward	AACCGAGAGGCTGAGACTAAC
	Reverse	GGAATGAAGGTGGCTGCTATG
Human *CXCL10*	Forward	TTCAAGGAGTACCTCTCTCTAG
	Reverse	CTGGATTCAGACATCTCTTCTC
Human *HLA-A*	Forward	TTGAGAGCCTACCTGGATGG
	Reverse	TGGTGGGTCATATGTGTCTTG
Human *HLA-B*	Forward	CTTCAAGAGCCTCTGGCATC
	Reverse	AGGGGTCACAGTGGACACA
Human *β-actin*	Forward	GGATGCAGAAGGAGATCACT
	Reverse	CGATCCACACGGAGTACTTG

Mouse *PSPH*	Forward	ACCGTCATCAGAGAAGAAG
	Reverse	CTTATGCCAGGAGTCAGAT
Mouse *CCL2*	Forward	AGCCAACTCTCACTGAAG
	Reverse	CTCTCCAGCCTACTCATTG
Mouse *CXCL10*	Forward	GGCTCGTCAGTTCTAAGTT
	Reverse	TGATGACACAAGTTCTTCCA
Mouse *β-actin*	Forward	CCAGGTCATCACTATTGGCAAC
	Reverse	TACGGATGTCAACGTCACAC

Lentiviral shRNA

shRNA	Vector		Sequences
Human sh*PSPH1*	pLKO.1-H-sh*PSPH1*	Forward	CCGGTGAGGACGCGGTGTCAGAAATCTCGAGATTTCTGACACCGCGTCCTCATTTTTG
		Reverse	AATTCAAAAATGAGGACGCGGTGTCAGAAATCTCGAGATTTCTGACACCGCGTCCTCA
Human sh*PSPH2*	pLKO.1-H-sh*PSPH2*	Forward	CCGGGGATAACGCCAAATGGTATATCTCGAGATATACCATTTGGCGTTATCCTTTTTG
		Reverse	AATTCAAAAAGGATAACGCCAAATGGTATATCTCGAGATATACCATTTGGCGTTATCC
Mouse sh*PSPH1*	pLKO.1-M-sh*PSPH1*	Forward	CCGGAGGCTGAAGTTCTACTTTAATCTCGAGATTAAAGTAGAACTTCAGCCTTTTTTG
		Reverse	AATTCAAAAAAGGCTGAAGTTCTACTTTAATCTCGAGATTAAAGTAGAACTTCAGCCT
Mouse sh*PSPH2*	pLKO.1-M-sh*PSPH2*	Forward	CCGGACGTTGCTGCAAAGCTCAATACTCGAGTATTGAGCTTTGCAGCAACGTTTTTTG
		Reverse	AATTCAAAAAACGTTGCTGCAAAGCTCAATACTCGAGTATTGAGCTTTGCAGCAACGT

Supplementary Table S4. Antibodies used in studies.

Name	Supplier	Cat no.	Clone no.
Rabbit Anti-Human PSPH	proteintech	14513-1-AP	
Rabbit Anti-Human MTHFD1L	proteintech	16113-1-AP	
Rabbit Anti-Human ALDH1L2	proteintech	21391-1-AP	
Rabbit Anti-Human ALDH1L1	proteintech	17390-1-AP	
Rabbit Anti-Human MAT2A	proteintech	55309-1-AP	
Rabbit Anti-Human MAT1A	proteintech	12395-1-AP	
Rabbit Anti-Human H3K27me3	Cell Signaling Technology	9733	C36B11
Rabbit Anti-Human Histone H3	Cell Signaling Technology	4499	D1H2
Rabbit Anti-Human p-STAT3^{Tyr705}	Cell Signaling Technology	9145	D3A7
Mouse Anti-Human STAT3	Cell Signaling Technology	9139	124H6
Mouse Anti-Human β-Actin	Abcam	ab14935	AC-15
Mouse Anti-Human CD68	Dako	M087629	PG-M1
Rabbit Anti-Human CD8a	Cell Signaling Technology	85336	D8Y8A
Rabbit Anti-Mouse CD8a	Cell Signaling Technology	98941	D4W2Z
Rabbit Anti-Mouse F4/80	Cell Signaling Technology	70076	D2S9R
Rat Anti-Mouse Ly6C	Abcam	ab15627	ER-MP20
PE-CF594 Rat Anti-Mouse Ly-6G	BD Biosciences	562700	1A8
Ly-6G/Ly-6C Monoclonal Antibody, FITC	eBioscience	11-5931-85	RB6-8C5
PC7-conjugated anti-mouse CD11b	Biolegend	101216	M1/70
BV 570 anti-mouse CD45 Antibody	Biolegend	103135	30-F11
BV421 anti-mouse Ly-6C Antibody	Biolegend	128032	HK1.4
AF700 anti-mouse CD11b Antibody	Biolegend	101222	M1/70
APC anti-mouse F4/80 Antibody	Biolegend	123116	BM8
PE anti-mouse CD8a Antibody	Biolegend	100708	53-6.7
FITC anti-mouse CD3 Antibody	Biolegend	100203	17A2

APC anti-mouse Perforin Antibody	Biolegend	154404	S16009B
PC7 anti-mouse Granzyme B Antibody	Biolegend	372214	QA16A02
Rat IgG2a isotype control antibody	Bioxcell	BP0089	2A3
Anti-mouse CD8a antibody	Bioxcell	BE0004	53-6.7
Anti-mouse PD-1 antibody	Bioxcell	BE0146	RMP1-14
HRP-conjugated goat anti-rabbit IgG	Cell Signaling Technology	7074	
HRP-conjugated goat anti-mouse IgG	Cell Signaling Technology	7076	

Supplementary Table S5. Reagents used in studies.

Name	Supplier	Cat no.
RPMI 1640 medium	Thermo Fisher Scientific	C11875500BT
DMEM	Thermo Fisher Scientific	C11995500BT
FBS	Gibco	10099-141
Penicillin	GENVIEW	AP231
Streptomycin	GENVIEW	AS325
Hepes	Sigma-Aldrich	H4034
DNase I	Sigma-Aldrich	DN25
Collagenase IV	Sigma-Aldrich	C5138
Hyaluronidase	Sigma-Aldrich	H1136
Collagenase XI	Sigma-Aldrich	C7657
DMSO	Merck Millipore	317275
Cultrex Basement Membrane Extract	R&D Systems	3432-005-01
Polyethylenimine Linear	Polysciences	24765
DAPI	Roche	10236276001
$GdCl_3$	Sigma-Aldrich	4399770
AG490	MCE	HY-12000
3-Deazaadenosine hydrochloride	MCE	HY-W013332A
N-Acetyl-L-cysteine	Sigma-Aldrich	A7250
S-(5′-Adenosyl)-L-methionine	Sigma-Aldrich	A7007
Recombinant Human TNF-α	R&D SYSTEMS	210-TA-010
Recombinant Human IL-1β	R&D SYSTEMS	201-LB-005
Recombinant Human IFN-γ	R&D SYSTEMS	285-IF-100
Human CXCL10 ELISA Kit	Invitrogen	CHC2363
Human CCL2 ELISA Kit	Invitrogen	88-7399-88
Human SAM ELISA Kit	MEIMIAN	MM-13267H1
Human SAH ELISA Kit	MEIMIAN	MM-13268H1
Human GSH/GSSG ELISA Kit	Beyotime	S0053
Dichlorofluorescein diacetate	Sigma-Aldrich	2044-85-1
Metformin	MCE	HY-17471A
CCK-8	Abcam	ab228554
Apoptosis analysis kit	eBioscience	88-8005-72
EnVision System	Dako	K5007
Opal 7-Color Automation IHC Kit	Perkinelmer	NEL801001KT
TRIzol Reagent	Life Techonology	AM9738
5X All-In-One RT Master Mix	abm	G486
SYBR Green Real-Time PCR Master Mix	TOYOBO	QPS-201
IntraPrep Permeabilization Reagent	Beckman Coulter	A07803